Highly Emissive Perylene Diimide-Based Metallacages and Their Host-Guest Chemistry for Information Encryption

Yali Hou,[†] Zeyuan Zhang,[†] Shuai Lu,[‡,‖] Jun Yuan,[§] Qiangyu Zhu,[#] Wei-Peng Chen,[$] Sanliang Ling,[⊥] Xiaopeng Li,[‡] Yan-Zhen Zheng,[$] Kelong Zhu,[§] Mingming Zhang,[*,†]

[†]State Key Laboratory for Mechanical Behavior of Materials, Shaanxi International Research Center for Soft Matter, School of Materials Science and Engineering, Xi'an Jiaotong University, Xi'an 710049, P. R. China

[‡] College of Chemistry and Environmental Engineering, Shenzhen University, Shenzhen 518055, P. R. China

[‖]College of Chemistry and Molecular Engineering, Zhengzhou University, Zhengzhou 450001, P. R. China

[§] School of Chemistry, Sun Yat-Sen University, Guangzhou 510275, P. R. China

[#]School of Chemistry and Chemical Engineering, Shanghai Jiao Tong University, Shanghai 200240, P. R. China

[$]Frontier Institute of Science and Technology (FIST), Xi'an Jiaotong University, Xi'an 710049, P. R. China

[⊥]Advanced Materials Research Group, Faculty of Engineering, University of Nottingham, Nottingham, NG7 2RD, United Kingdom

Supporting Information

1. Materials and methods

All reagents and deuterated solvents were used as purchased without further purification. Compounds **8**,[S1] **3**[S2] and **6**[S1] were prepared according to the literature procedures. NMR spectra were recorded on a Bruker Avance 400 or 600 MHz spectrometer. ^{1}H NMR chemical shifts were recorded relative to residual solvent signals. ^{31}P{^{1}H} NMR chemical shifts were referenced to an external unlocked sample of 85% H_3PO_4 (δ 0.0). Mass spectra were recorded on a Micromass Quattro II triple-quadrupole mass spectrometer using electrospray ionization with a MassLynx operating system. The UV-vis experiments were conducted on a Lambd 950 absorption spectrophotometer. The fluorescent experiments were conducted on an Edinburgh FLS9 or a Hitachi F-7000 fluorescence spectrophotometer. X-ray diffraction analysis was conducted on a Bruker SMART APEX II diffractometer at 108 K with graphite-monochromated Mo K_α radiation (λ = 0.71073 Å) or a Bruker D8 VENTURE PHOTON III MetalJet, in which crystals were frozen in paratone oil inside a cryoloop under a cold stream of N_2. An empirical absorption correction using SADABS was applied for all data. The structures were solved and refined to convergence on F2 for all independent reflections by the full-matrix least squares method using the OLEX2 1.2. ^{1}H NMR titration experiments were performed by the addition of different amount of metallacages into the CD_3CN solution of polyaromatic guests and the concentration of the guests was fixed to be 0.5 mM. The data was fitted according to the following equation:

$$\delta = (\Delta\delta_{max}/[G]_0)\,(0.5[H] + 0.5\,([G]_0+1/K_a) - (0.5([H]^2+(2[H](1/K_a - [G]_0)) + (1/K_a + [G]_0)^2)^{0.5}))$$

Where δ is the ^{1}H NMR chemical shifts of guest molecules upon the addition of metallacages, $\Delta\delta_{max}$ is the maximum chemical shift change when the guests are totally complexed, $[G]_0$ is the fixed concentration of guests (0.5 mM), [H] is the concentration of the metallacages.[S3]

2. Synthetic procedures and characterization data

*2.1 Synthesis of compound **8***

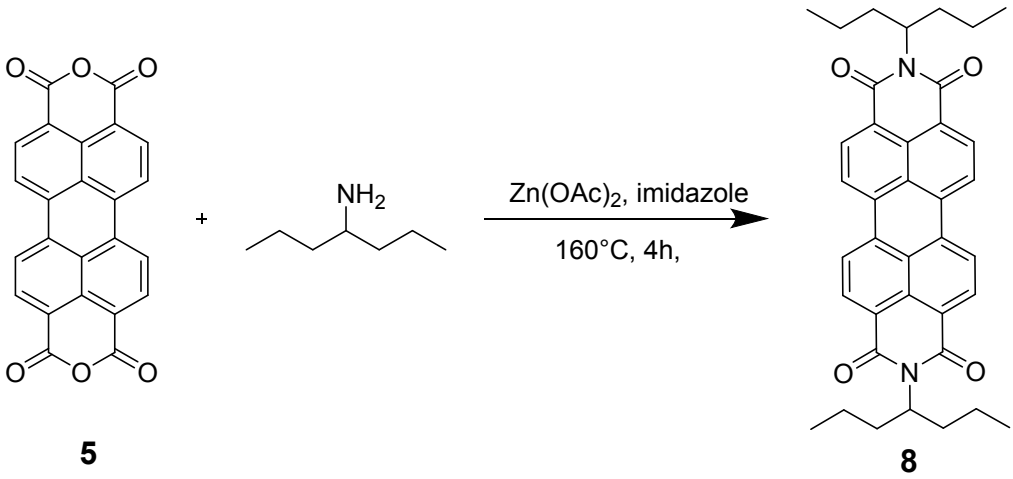

5 **8**

Compound **5** (1.00 g, 2.54 mmol), $Zn(OAc)_2$ (0.77 g, 4.08 mmol) and imidazole (8.37 g, 102 mmol) were added in 4-heptylamine (0.96 g, 8.40 mmol) under a N_2 atmosphere and the whole system was stirred at 165 ^{o}C for 4 h. After being cooled to room temperature, the reaction mixture was filtrated and

the residue was washed with methanol. The crude product was purified by flash column chromatography (CH_2Cl_2) to give compound **8** (1.30 g, 86%) as a red solid. ^{1}H NMR (400 MHz, $CDCl_3$, 295 K) δ 8.61–8.66 (m, 8H), 5.20–5.27 (m, 2H), 2.18–2.33 (m, 4H), 1.79–1.87 (m, 4H), 1.24–1.43 (m, 8H), 0.93 (t, J = 7.3 Hz, 12H). The ^{1}H NMR spectrum of **8** matches well with reported results.[S1]

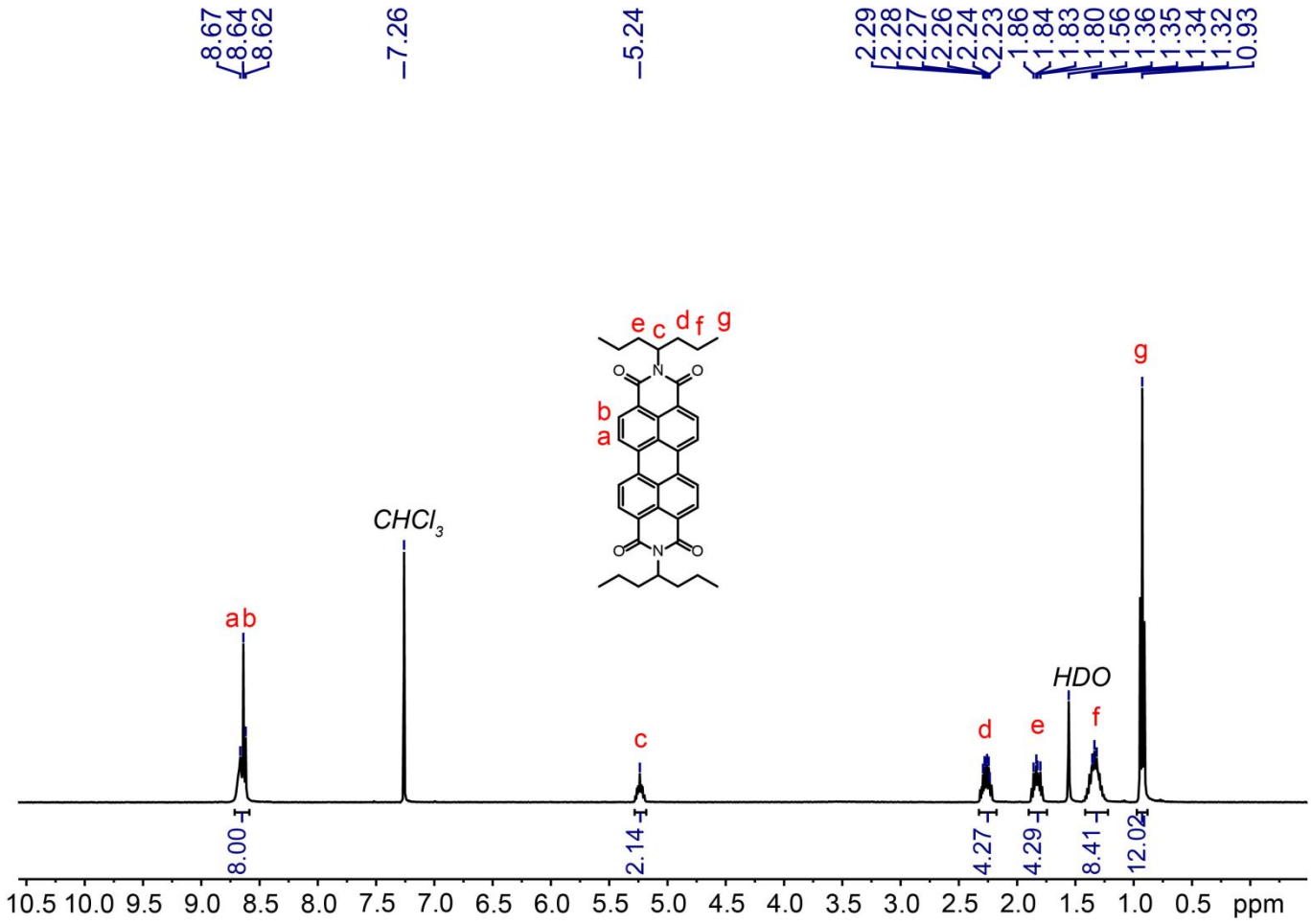

Figure S1. ^{1}H NMR spectrum ($CDCl_3$, 400 MHz, 295 K) recorded for **8**.

2.2 Synthesis of compound ***6***

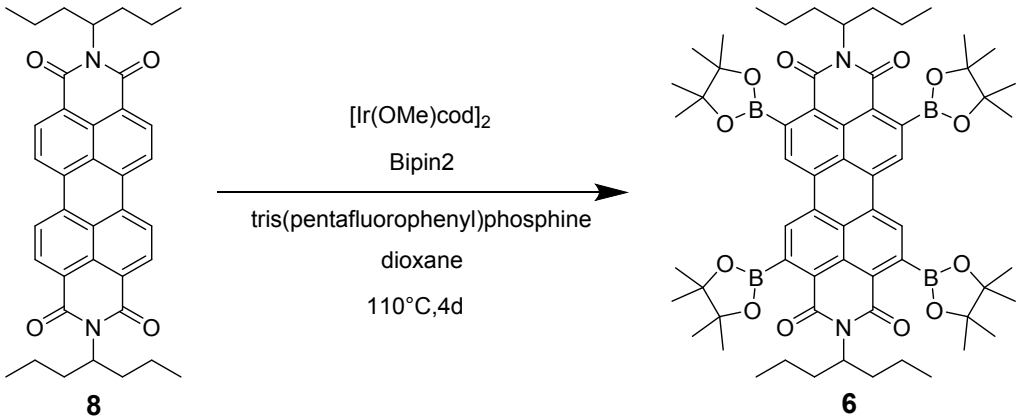

8 **6**

A mixture of compound **8** (266 mg, 0.45 mmol), $[Ir(OMe)cod]_2$ (29.8 mg, 45.0 mol), tris(pentafluorophenyl)phosphine (0.10 mg, 0.19 mmol), and bis(pinacolato)diboron (1.03 g, 4.04 mmol)

in 10 mL of dioxane was stirred under nitrogen at 120 °C for 4 days. After being cooled to room temperature, the solvent was removed under reduced pressure. The residue was purified by flash column chromatography (dicholromethane : ethyl acetate = 1:1) to give compound **6** (0.30 g, 61%) as a red solid. ^{1}H NMR (400 MHz, $CDCl_3$, 295 K) δ 8.52 (s, 4H), 5.04–5.13 (m, 2H), 2.15–2.24 (m, 4H), 1.75–1.84 (m, 4H), 1.54 (s, 48H), 1.31–1.39 (m, 8H), 0.91 (t, *J* =7.3 Hz, 12H). The ^{1}H NMR spectrum of **6** matches well with reported results.[S1]

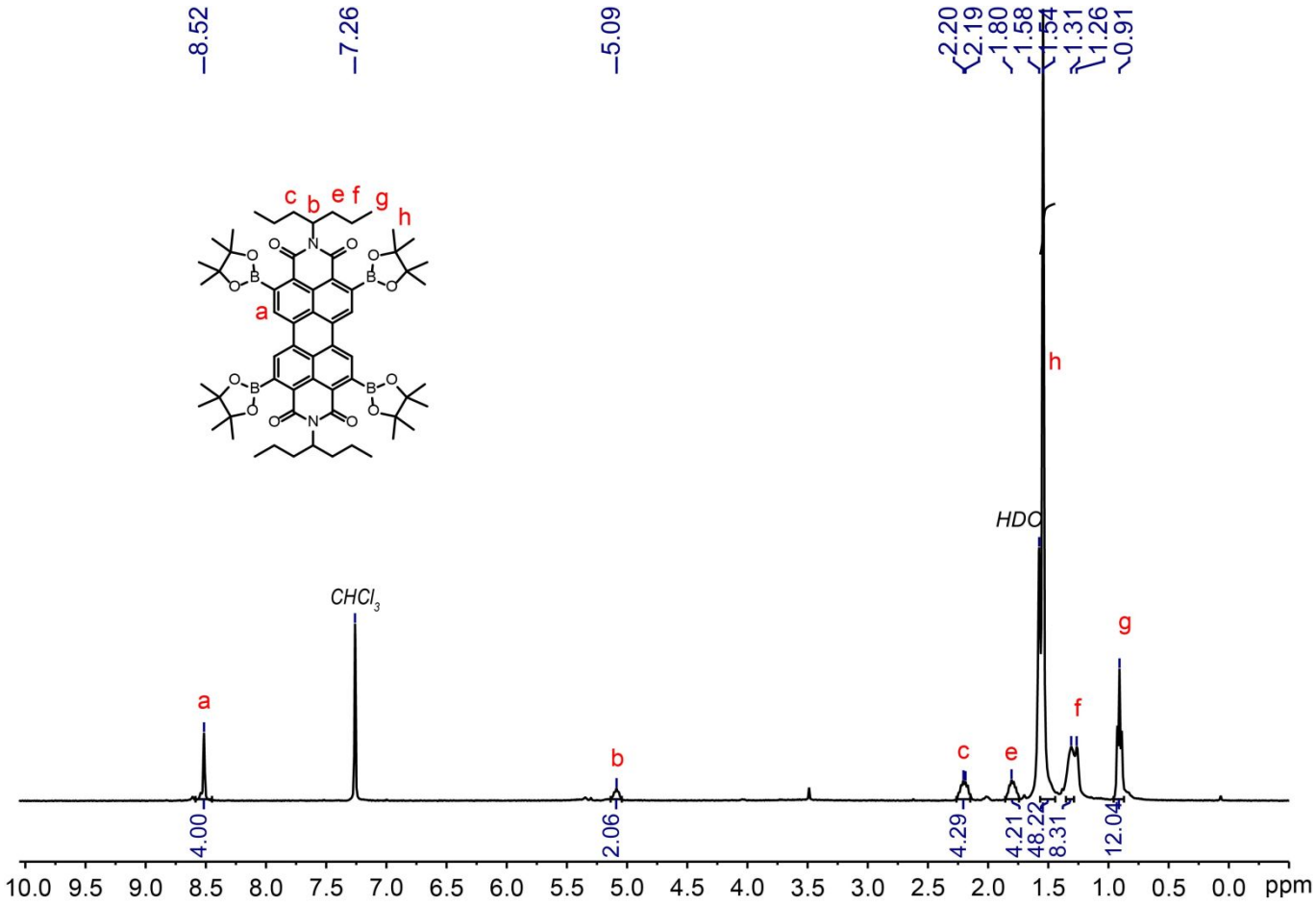

Figure S2. ^{1}H NMR spectrum (400 MHz, $CDCl_3$, 295 K) recorded for **6**.

*2.3 Synthesis of ligand **1***

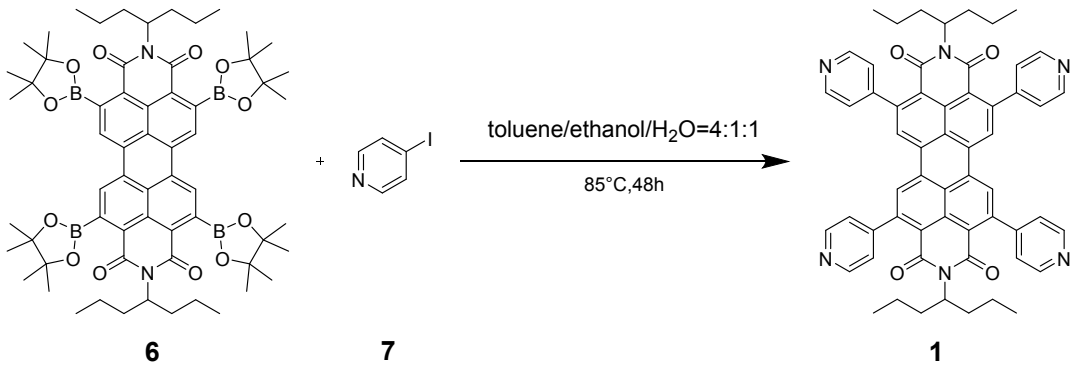

To compound **6** (0.30 g, 0.28 mmol), 4-pyridylboronic acid (0.68 g, 3.36 mmol), anhydrous Cs_2CO_3 (1.90 g, 13.8 mmol) and $Pd(PPh_3)_4$ (63.6 mg, 0.05 mmol) in toluene (28.0 mL), H_2O (7.0 mL) and ethanol (7.0 mL) were added. Then the reaction mixture was stirred at 85 °C for 48 h under nitrogen atmosphere. After being cooled to room temperature, the product was concentrated to give a crude product which was purified by flash column chromatography with CH_2Cl_2:CH_3OH (50:1, *v*/*v*) as the eluent to afford compound **1** (0.15 g, 60%) as an orange powder. M.P. 451.39~451.97 °C. ^{1}H NMR (400 MHz, $CDCl_3$, 295 K) δ 8.77 (d, *J* = 4.8 Hz, 8H), 8.31 (s, 4H), 7.35 (d, *J* = 4.8 Hz, 8H), 4.88–4. 95 (m, 2H), 1.95–2.04 (m, 4H), 1.59–1.67 (m, 4H), 1.22–1.27 (m, 8H), 0.88 (t, *J* = 7.3 Hz, 12H). ^{13}C NMR (151 MHz, $CDCl_3$, 295 K) 162.90, 150.16, 149.78, 145.29, 132.70, 130.87, 126.78, 126.02, 122.71,121.54,54.56, 34.00, 20.03, 13.97. ESI-HR-MS: *m/z* 895.3967 [**1** + H]$^+$, calcd. for $[C_{58}H_{50}N_6O_4]^+$, 895.3894.

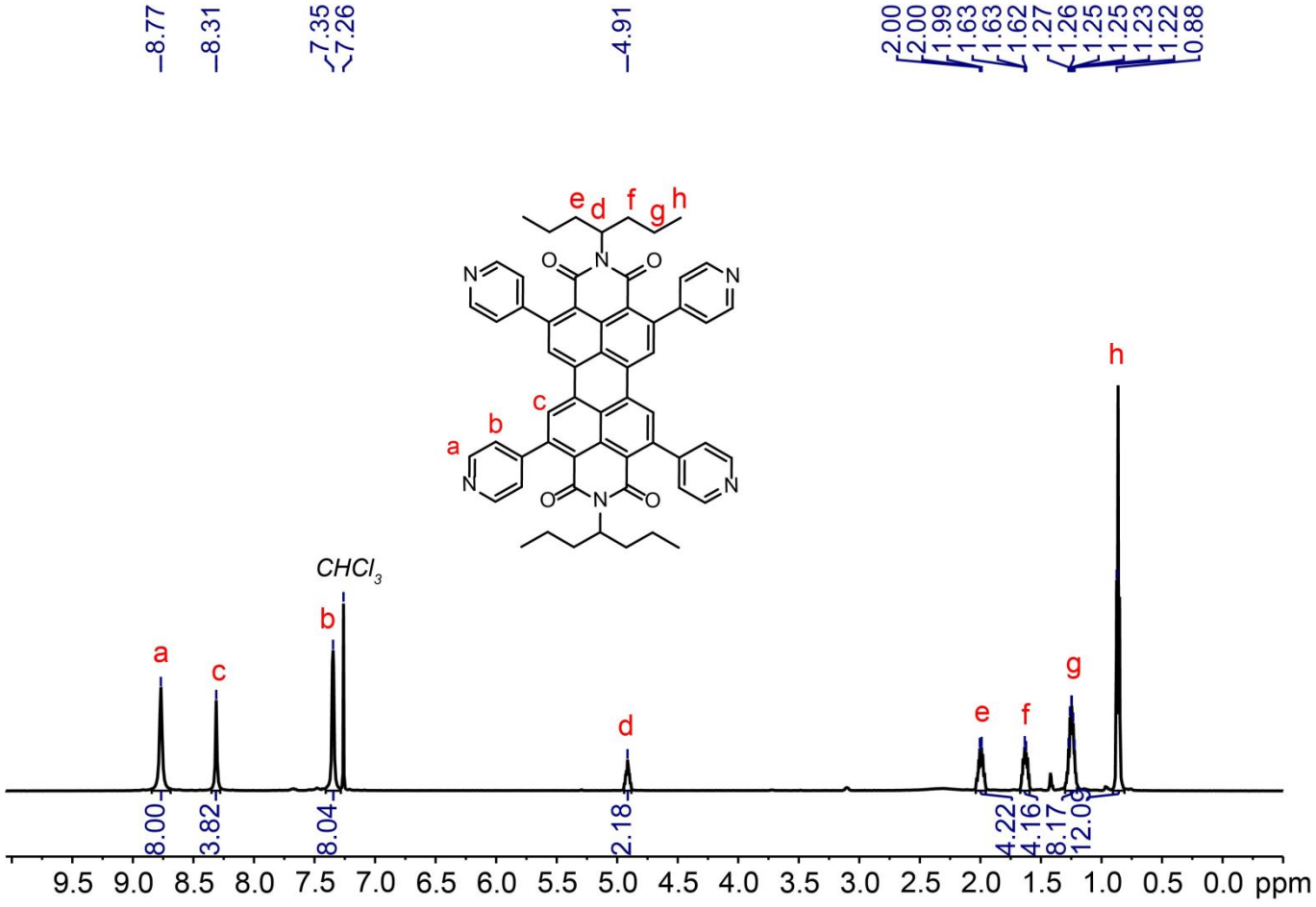

Figure S3. ^{1}H NMR spectrum (400 MHz, $CDCl_3$, 295 K) recorded for **1**.

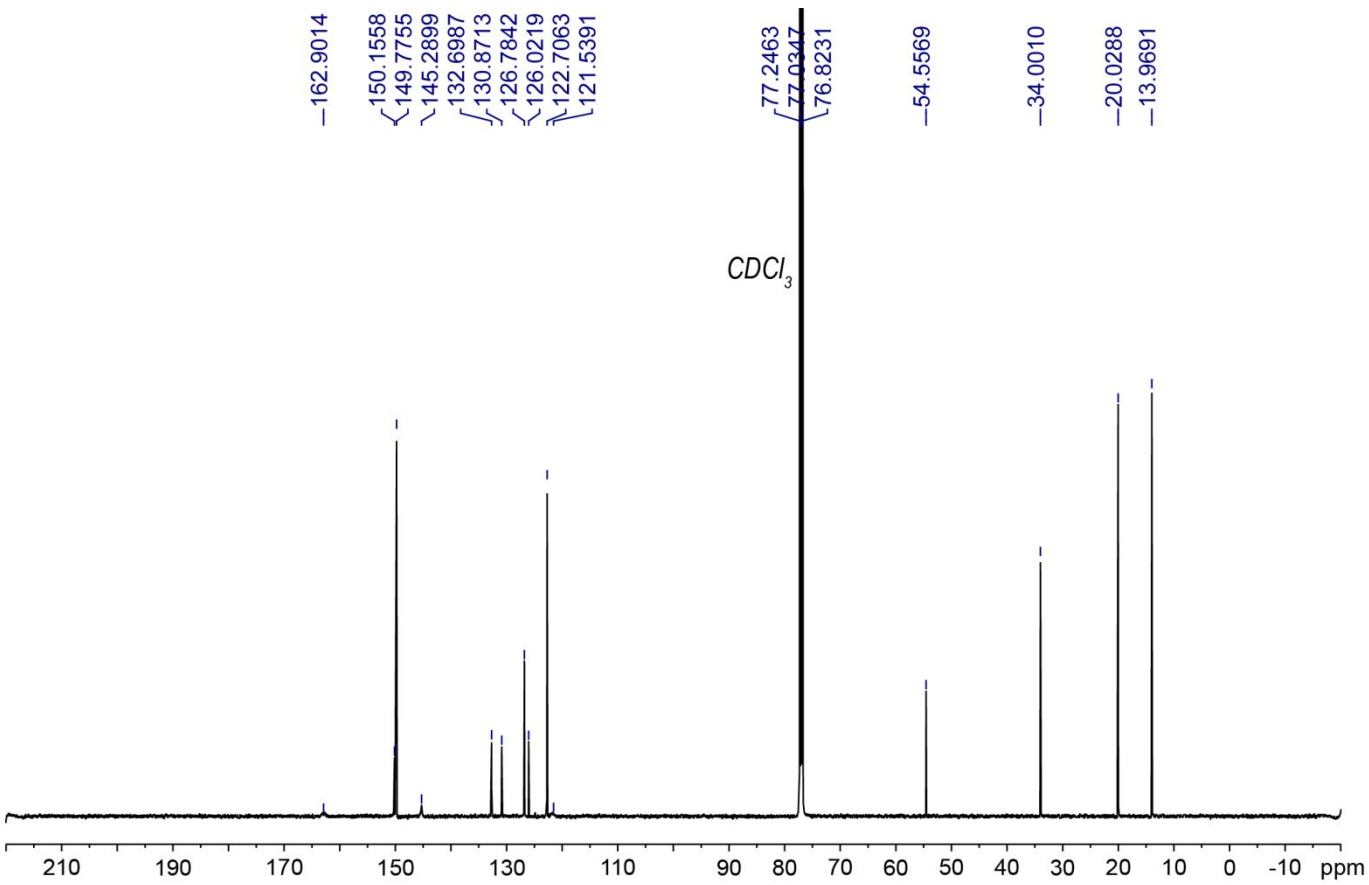

Figure S4. ^{13}C NMR spectrum (151 MHz, $CDCl_3$, 295 K) recorded for **1**.

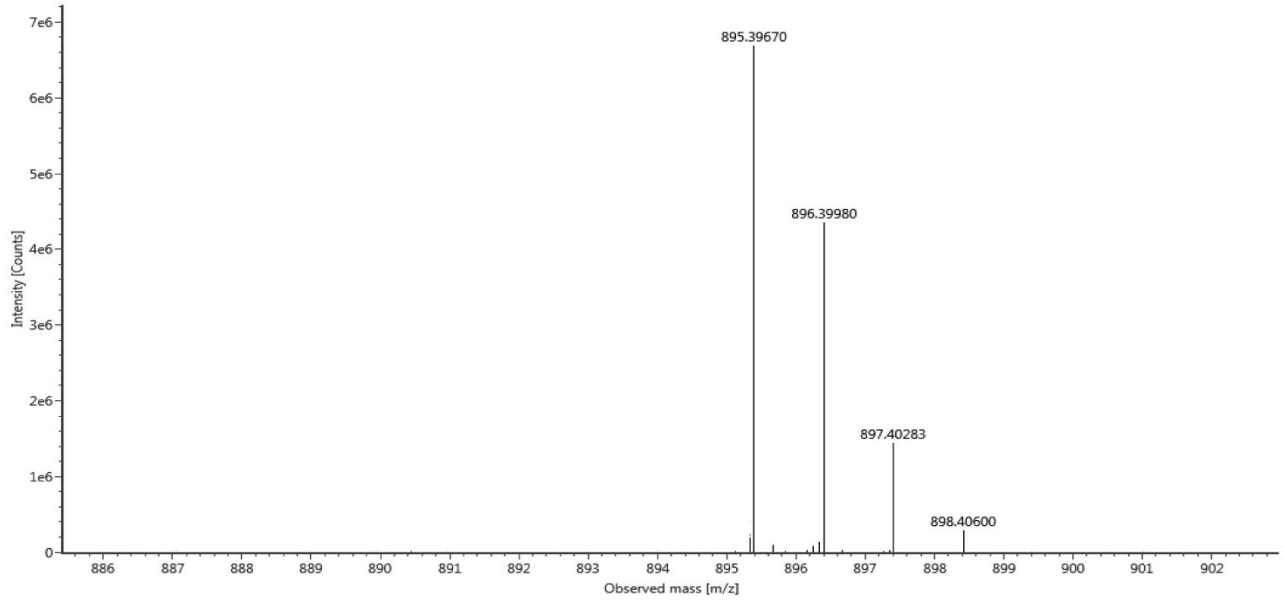

Figure S5. ESI-HR-MS spectrum of **1**.

2.4 Self-assembly of metallacycle ***4a***

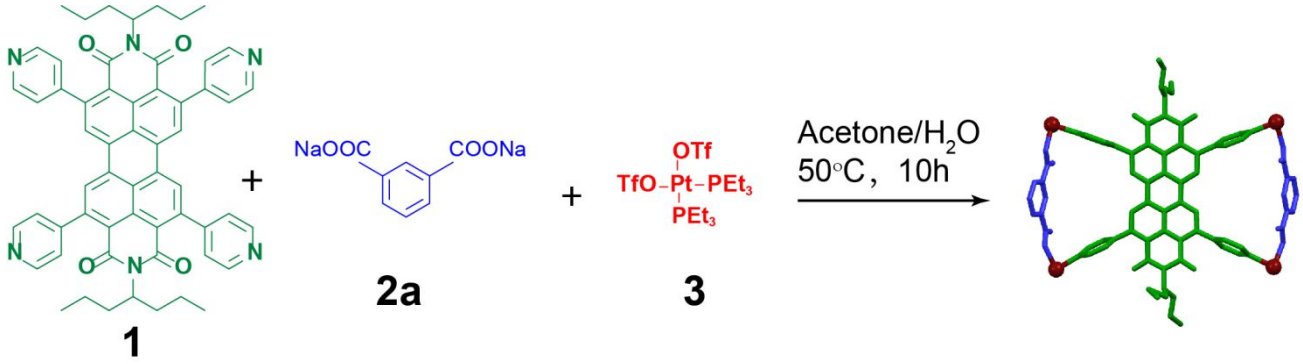

Figure S6. Self-assembly of metallacycle **4a**.

1 (3.12 mg, 3.48 μmol), sodium isophthalate **2a** (1.46 mg, 6.96 μmol), and *cis*-$(PEt_3)_2Pt(OTf)_2$ (10.17 mg, 13.92 μmol) were mixed in a 1:2:4 molar ratio and dissolved in acetone/water (5.0 mL, 4:1, *v*/*v*). The whole reaction mixture was heated at 50 °C for 10 h and then cooled to room temperature. The solvent was removed by nitrogen flow. The residue was redissolved in CH_3CN (1.0 mL) and filtered, and then the filtrate was poured into ethyl ether (10.0 mL) to give a precipitate, which was collected by centrifugation to give **4a** (11.47 mg, 93%) as an orange powder. ^{1}H NMR (400 MHz, CD_3CN, 295 K) δ 8.86 (d, J = 4.5 Hz, 8H), 8.44 (s, 4H), 8.21 (s, 2H), 7.94 (dd, J = 7.7, 1.6 Hz, 4H), 7.53 (d, J = 4.5 Hz, 8H), 7.32 (t, J = 7.7 Hz, 2H), 4.77–4.81 (m, 2H), 0.81 (t, J = 7.3 Hz, 12H). ^{31}P{^{1}H} NMR (121.4 MHz, CD_3CN, 295 K): 5.42 ppm (d, $^2J_{P\text{-}P}$ =15.8 Hz, ^{195}Pt satellites, $^1J_{Pt\text{-}P}$ = 2600 Hz), –0.56 ppm (d, $^2J_{P\text{-}P}$ =15.8 Hz, ^{195}Pt satellites, $^1J_{Pt\text{-}P}$ = 2600 Hz); ESI-TOF-MS: *m*/*z* 736.9174 [**4a** – 4OTf]$^{4+}$, 1032.2203 [**4a** – 3OTf]$^{3+}$.

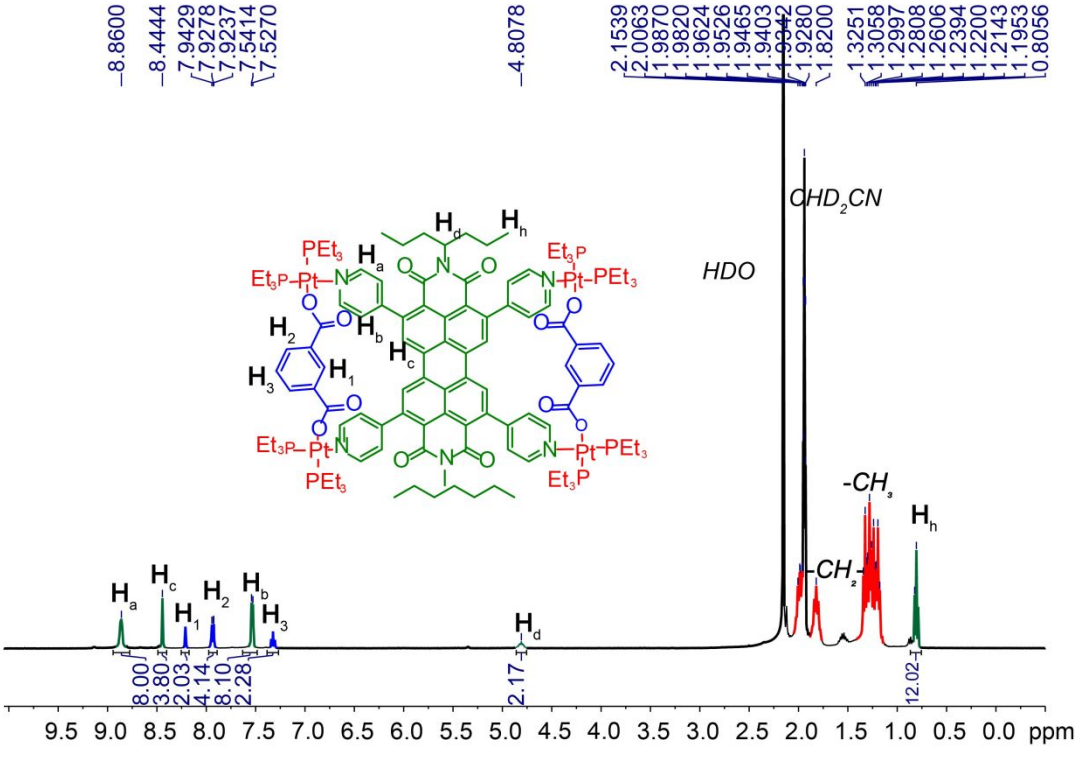

Figure S7. ^{1}H NMR spectrum (400 MHz, CD_3CN, 295 K) recorded for **4a**.

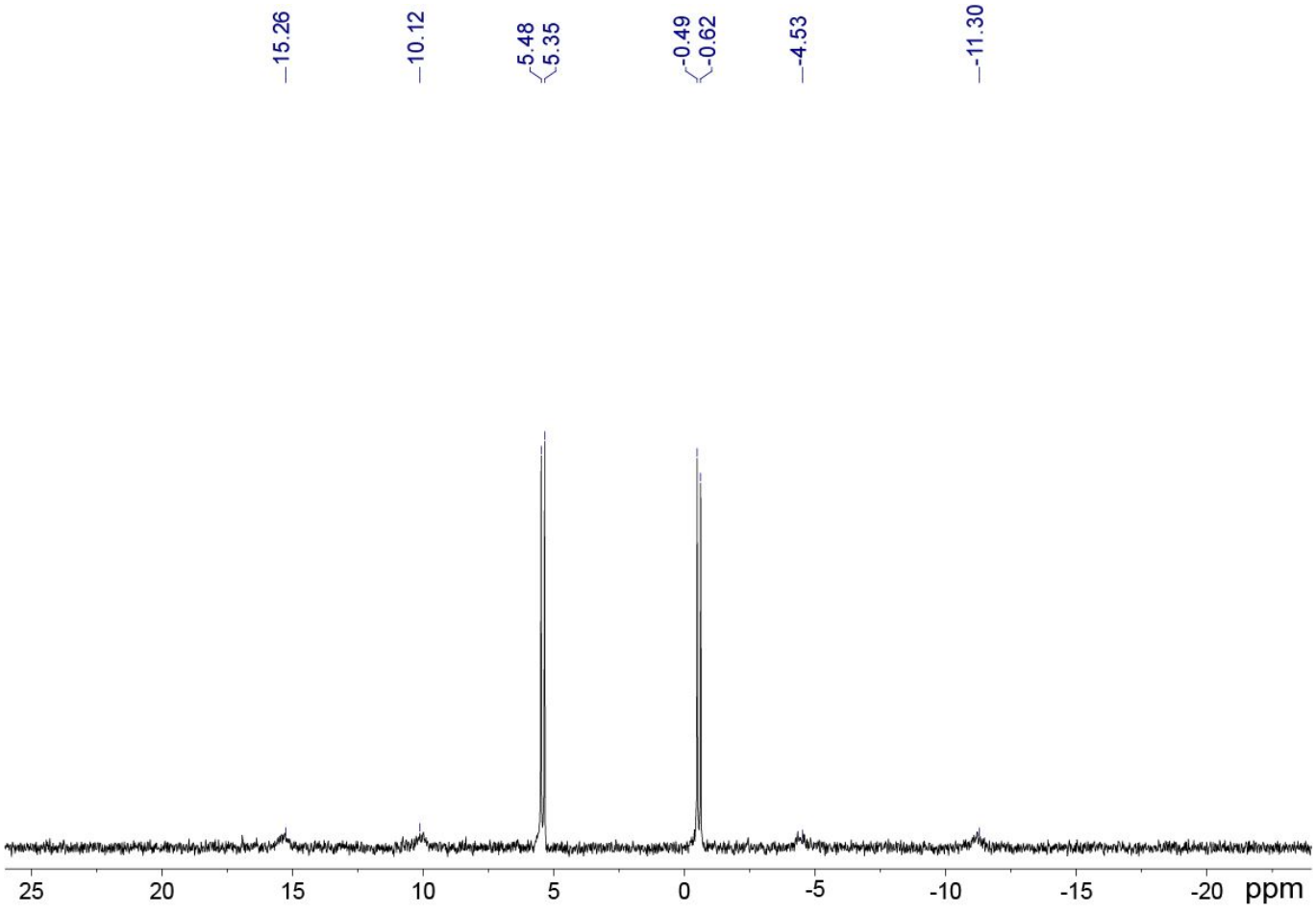

Figure S8. $^{31}P\{^{1}H\}$ NMR spectrum (121.4 MHz, CD_3CN, 295 K) recorded for **4a**.

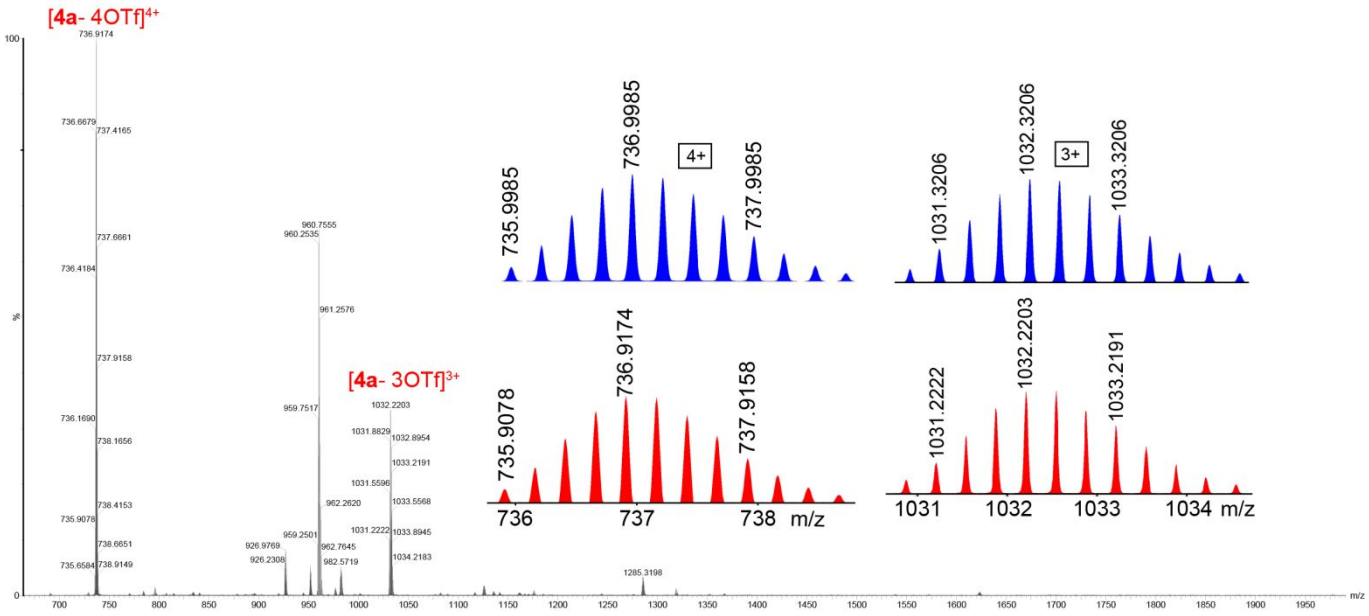

Figure S9. ESI-TOF-MS spectrum of **4a**.

*2.5 Self-assembly of metallacage **4b***

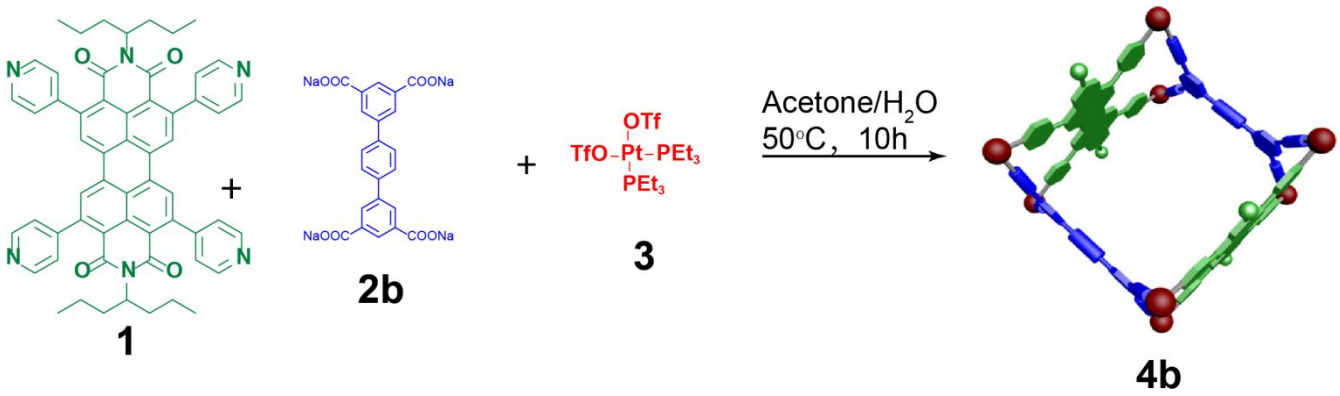

Figure S10. Self-assembly of metallacage **4b**.

1 (5.0 mg, 5.59 μmol), tetracarboxylate ligand **2b** (2.76 mg, 5.59 μmol), and *cis*-$(PEt_3)_2Pt(OTf)_2$ (16.30 mg, 22.34 μmol) were mixed in a 1:1:4 molar ratio and dissolved in acetone/water (5.0 mL, 4:1, *v*/*v*). The whole reaction mixture was heated at 50°C for 10 h and then cooled to room temperature. The solvent was removed by nitrogen flow. The residue was redissolved in CH_3CN (1.0 mL) and filtered, and the filtrate was poured into ethyl ether (10.0 mL) to give a precipitate, which was collected by centrifugation to give **4b** (19.0 mg, 94%) as an orange powder. ^{1}H NMR (400 MHz, CD_3CN, 295 K) δ 8.98–8.90 (m, 8H), 8.67–8.69 (m, 8H), 8.37 (s, 8H), 8.25 (d, J = 9.8 Hz, 12H), 7.72 (s, 8H), 7.61 (d, J = 5.3 Hz, 8H), 7.34 (d, J = 5.2 Hz, 8H), 4.71–4.79 (m, 4H), 0.76 (t, J = 7.3 Hz, 24H). ^{31}P{^{1}H} NMR (121.4 MHz, CD_3CN, 295 K): 5.14 ppm (d, $^2J_{P\text{-}P}$ =15.8 Hz, ^{195}Pt satellites, $^1J_{Pt\text{-}P}$ = 2600 Hz), –0.41 ppm (d, $^2J_{P\text{-}P}$ =15.8 Hz, ^{195}Pt satellites, $^1J_{Pt\text{-}P}$ = 2600 Hz). ESI-TOF-MS: *m/z* 1057.2615 [**4b** – 6OTf]$^{6+}$, 1298.5774 [**4b** – 5OTf]$^{5+}$, 1660.4084 [**4b** – 4OTf]$^{4+}$ and 2263.5923 [**4b** – 3OTf]$^{3+}$.

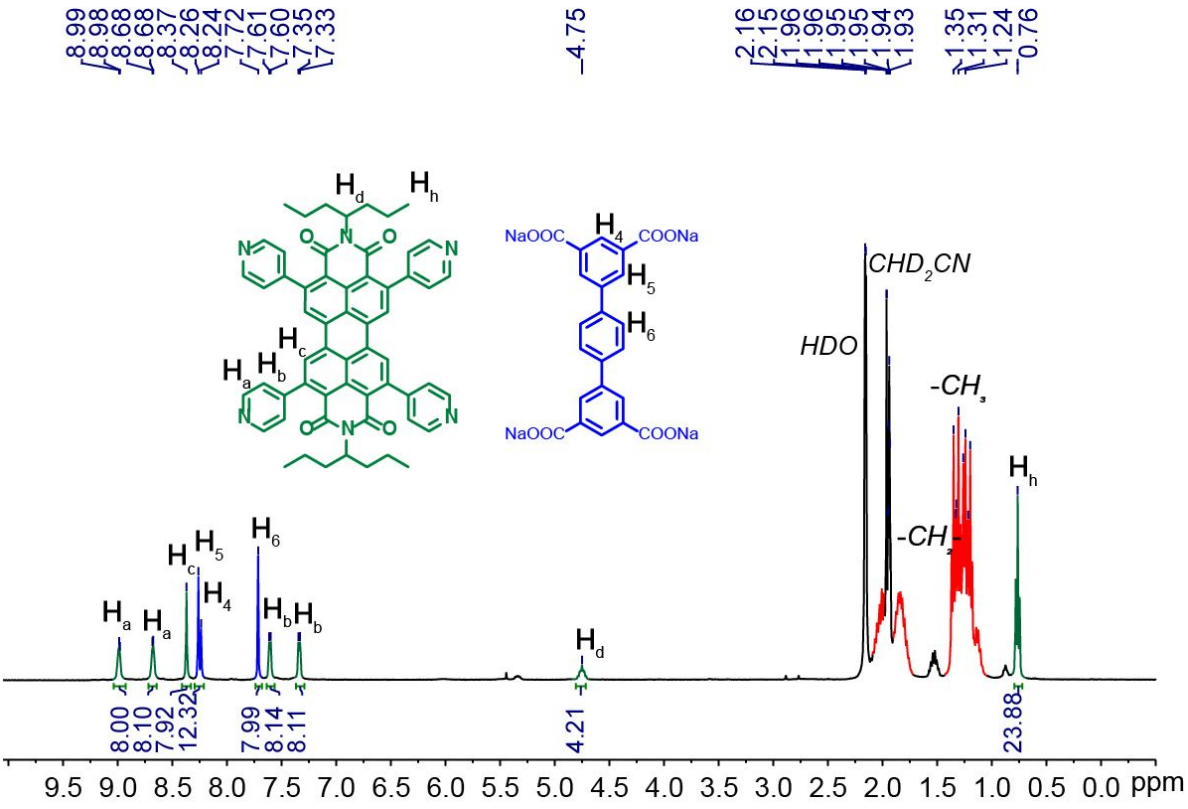

Figure S11. ^{1}H NMR spectrum (400 MHz, CD_3CN, 295 K) recorded for **4b**.

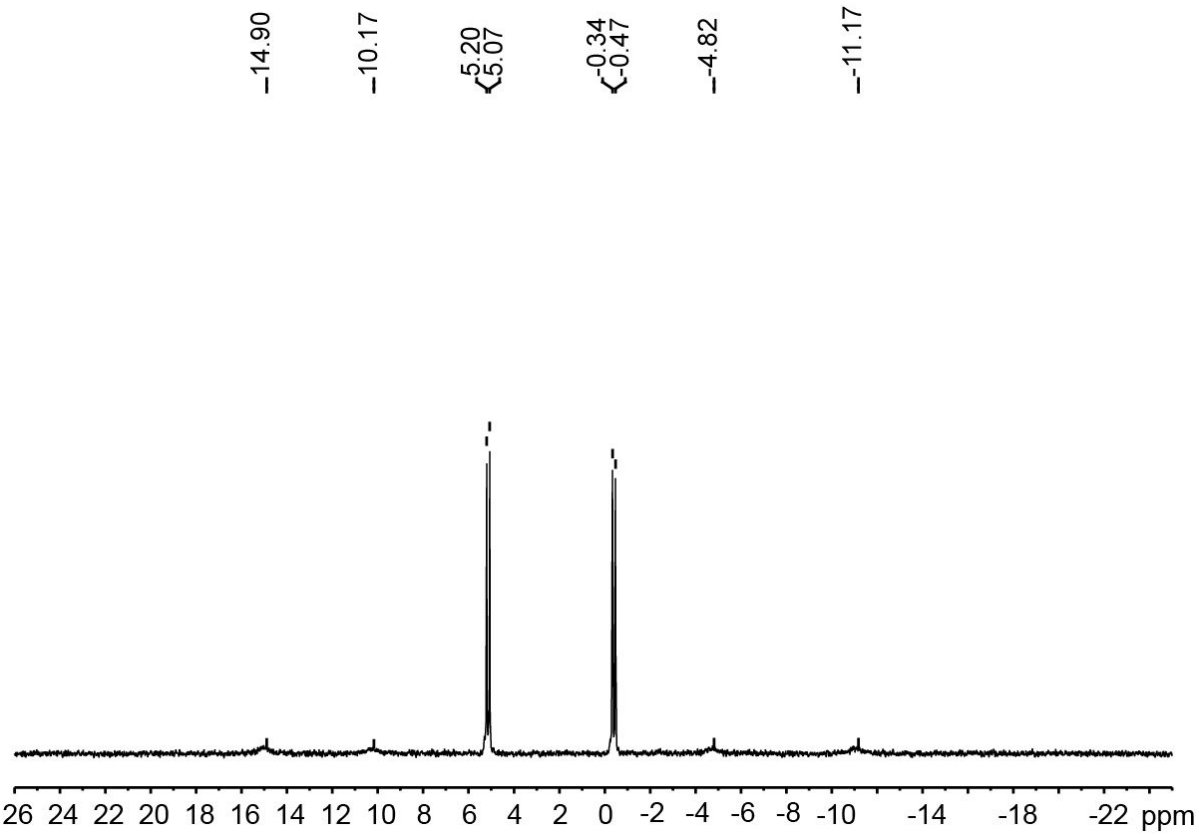

Figure S12. $^{31}P\{^{1}H\}$ NMR spectrum (121.4 MHz, CD_3CN, 295 K) recorded for **4b**.

*2.6 Self-assembly of metallacage **4c***

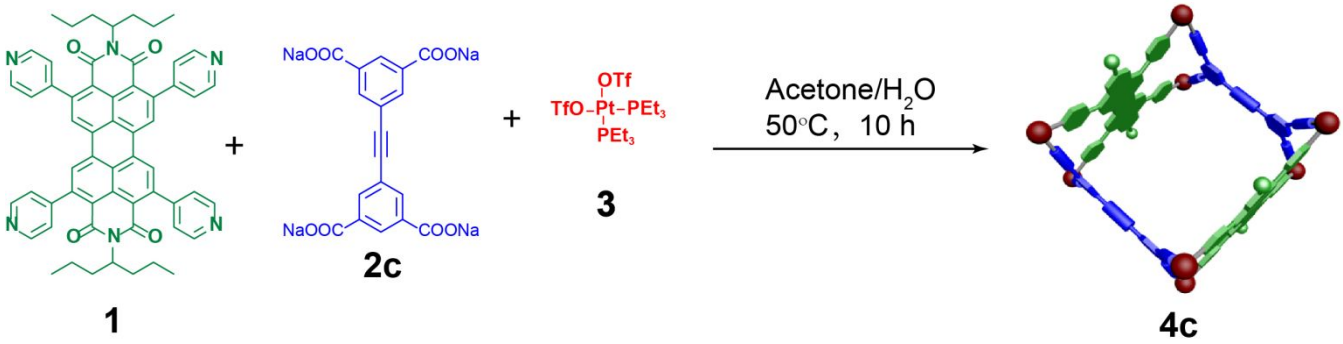

Figure S13. Self-assembly of metallacage **4c**.

1 (5.0 mg, 5.59 μmol), tetracarboxylate ligand **2c** (2.47 mg, 5.59 μmol), and *cis*-$(PEt_3)_2Pt(OTf)_2$ (16.30 mg, 22.34 μmol) were mixed in a 1:1:4 molar ratio and dissolved in acetone/water (5.0 mL, 4:1, *v*/*v*). The whole reaction mixture was heated at 50°C for 10 h and then cooled to room temperature. The solvent was removed by nitrogen flow. The residue was redissolved in CH_3CN (1.0 mL) and filtered, and the filtrate was poured into ethyl ether (10.0 mL) to give a precipitate, which was collected by centrifugation to give **4c** (18.35 mg, 92%) as an orange powder. ^{1}H NMR (400 MHz, CD_3CN, 295 K) δ 8.96–8.98 (m, 8H), 8.72–8.74 (m, 8H), 8.36 (s, 8H), 8.22 (s, 4H), 8.12 (d, J = 1.0 Hz, 8H), 7.58 (d, J = 5.0 Hz, 8H), 7.36 (d, J = 5.1 Hz, 8H), 4.71–4.79 (m, 4H), 0.76 (t, J = 7.3 Hz, 24H). $^{31}P\{^{1}H\}$ NMR (121.4 MHz, CD_3CN,

295 K): 5.22 ppm (d, $^{2}J_{P\text{-}P}$ =15.8 Hz, ^{195}Pt satellites, $^{1}J_{Pt\text{-}P}$ = 2591.89 Hz), –0.51 ppm (d, $^{2}J_{P\text{-}P}$ =15.8 Hz, ^{195}Pt satellites, $^{1}J_{Pt\text{-}P}$ = 2591.89 Hz). ESI-TOF-MS: *m/z* 1277.7677 [**4c** – 5OTf]$^{5+}$, 1634.4457 [**4c** – 4OTf]$^{4+}$ and 2228.9094 [**4c** – 3OTf]$^{3+}$.

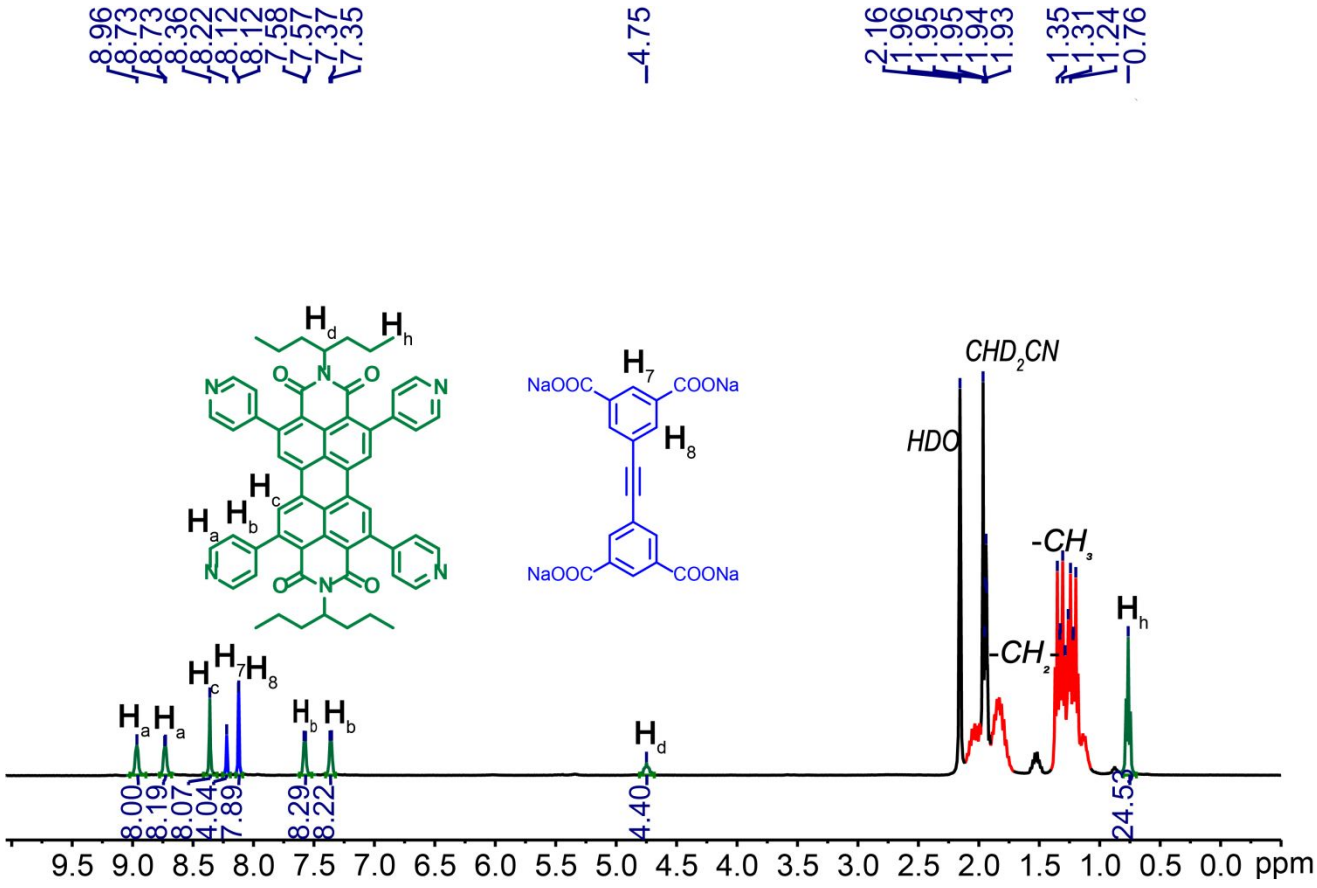

Figure S14. ^{1}H NMR spectrum (400 MHz, CD_3CN, 295 K) recorded for **4c**.

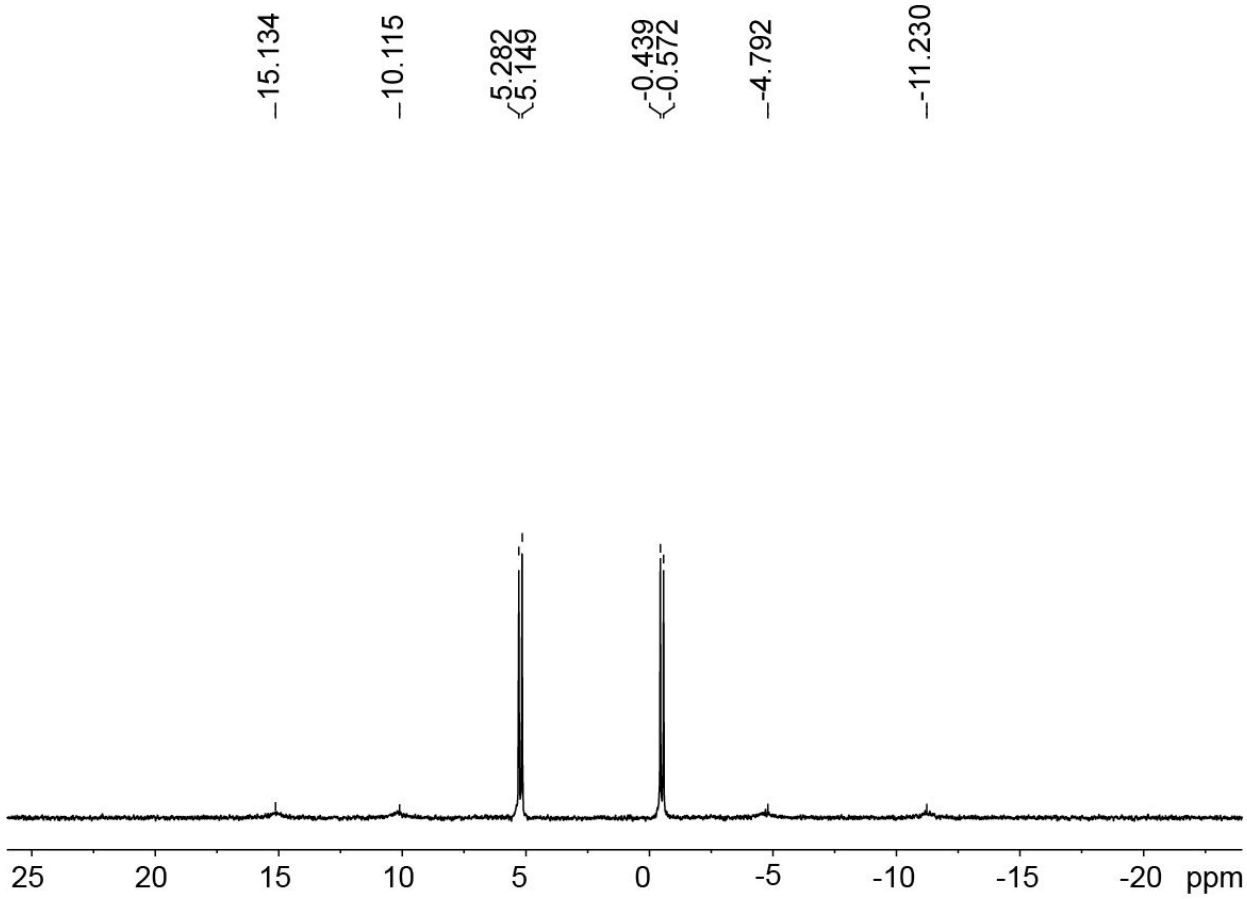

Figure S15. $^{31}P\{^{1}H\}$ NMR spectrum (121.4 MHz, CD_3CN, 295 K) recorded for **4c**.

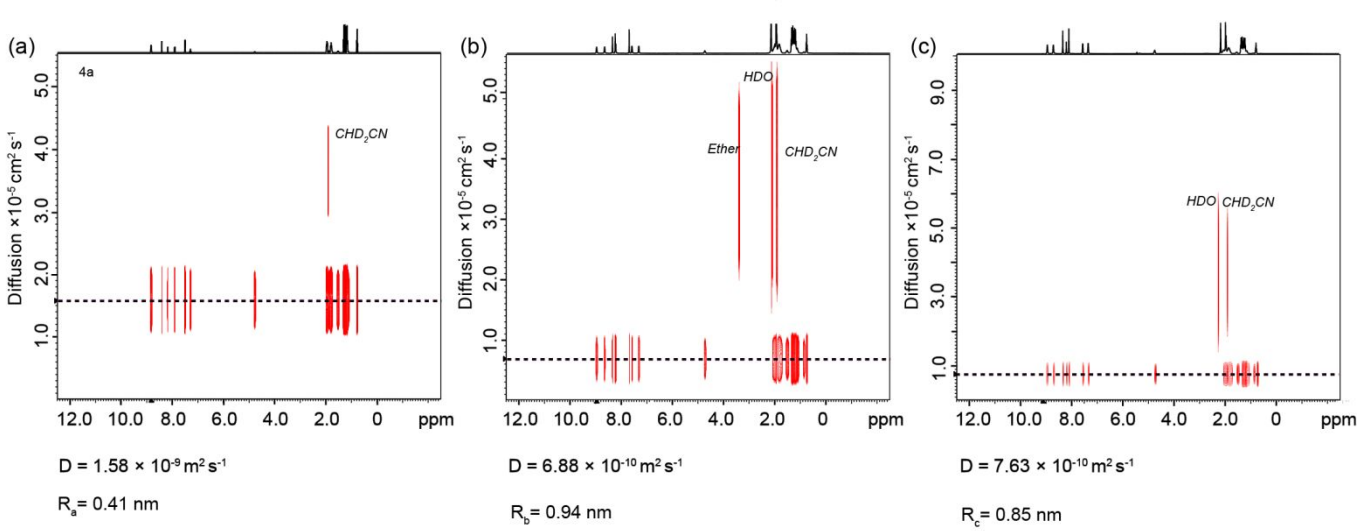

Figure S16. 2D ^{1}H DOSY spectra (400 MHz, CD_3CN, 295 K) recorded for (a) metallacycle **4a**, metallacages (b) **4b** and (c) **4c**.

3. X-ray structure determination

*Table S1. Crystallographic data and refinement details for compounds **4a**, **4b** and **4c***

Compound	**4a**	**4b**	**4c**
Empirical formula	$C_{125}H_{178}F_9N_6O_{21}P_8Pt_4S_3$	$C_{268}H_{374}F_{12}N_{12}O_{40}P_{16}Pt_8S_4$	$C_{278}H_{398}F_{24}N_{14}O_{58}P_{16}Pt_8S_8$
Fw	3396.02	6816.25	6816.25
Crystal system	Triclinic	Triclinic	Triclinic
Space group	*P*-1	*P*-1	*P*-1
a /Å	15.0681(5)	20.8686 (12)	21.295(6)
b /Å	23.3192(6)	23.3807 (15)	24.991(6)
c /Å	28.0394(7)	26.270 (2)	27.539(7)
α /°	72.453(2)	107.418 (4)	71.721(3)
β /°	77.385(2)	113.195 (2)	70.657(3)
γ /°	78.928(2)	94.271(3)	71.100(3)
V /Å^3	9082.5(5)	10967.6(13)	12728(6)
Z	2	1	1
D_{calc}/g cm^{-3}	1.242	1.032	0.996
F (000)	3398.0	3422.0	3836.0
μ /mm^{-1}	4.956	3.940	2.326
θ max	61.018	59.981	24.232
Independent reflns	27380	31822	23105
Reflns [$I > 2\sigma(I)$]	40437	48184	40147
R_1; wR_2 [$I > 2\sigma(I)$]	0.1098; 0.2264	0.1181; 0.3940	0.0824; 0.2797

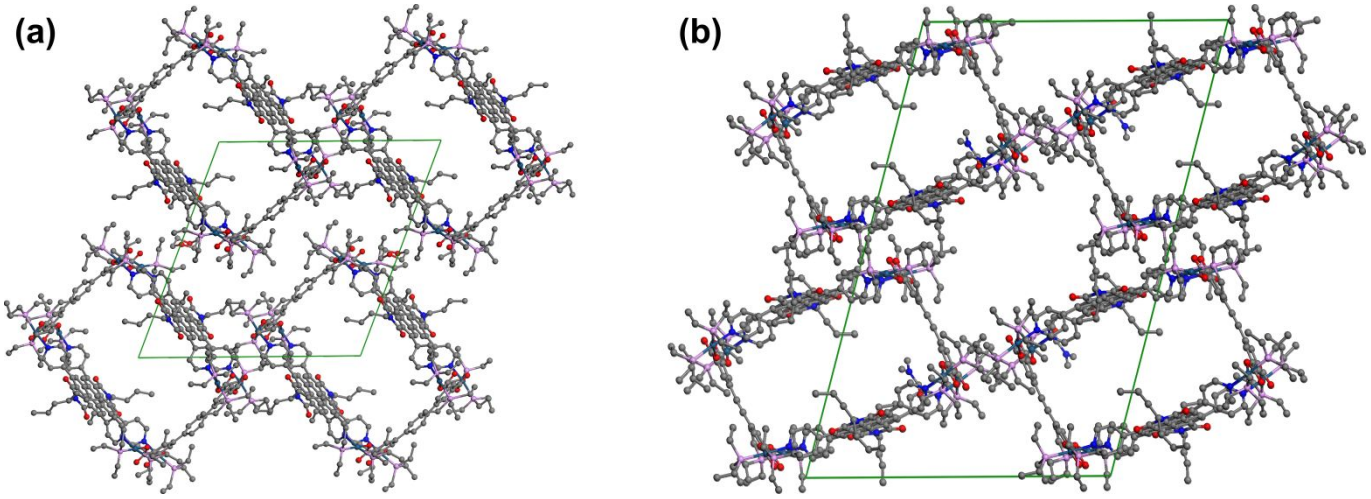

Figure S17.Packing mode of crystal structures of (a) **4b** and (b) **4c**. Hydrogen atoms, counterions and solvent molecules were omitted for clarity.

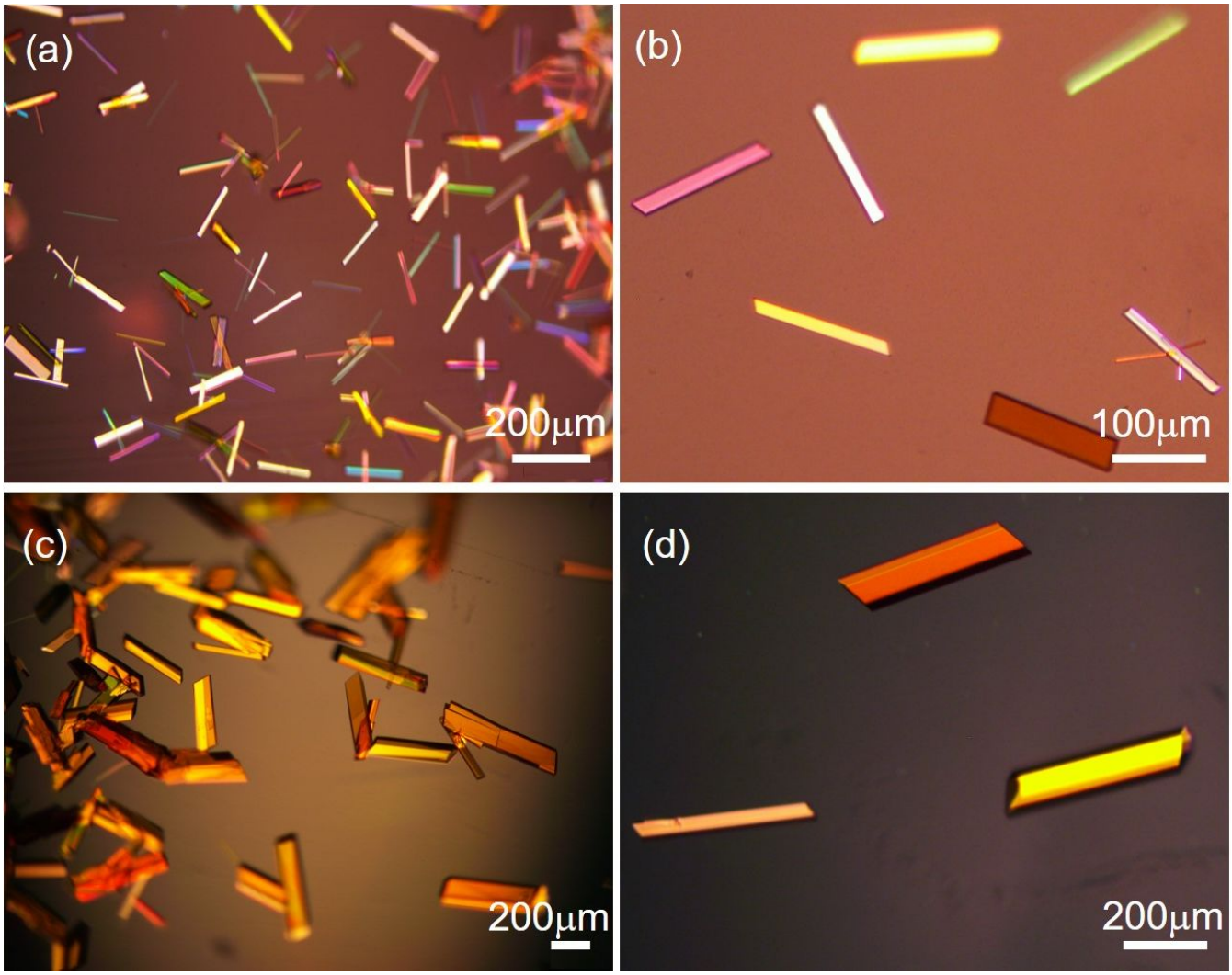

Figure S18. Optical images of crystals of metallacages (a, b) **4b** and (c, d) **4c**.

4. Measurements of absolute fluorescence quantum yields

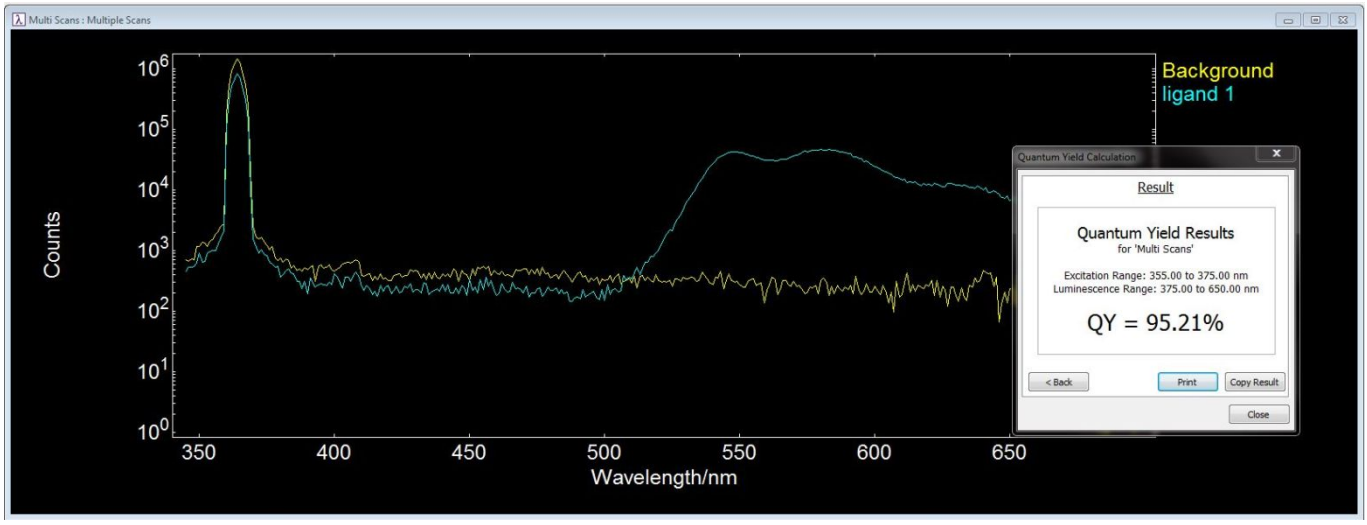

Figure S19. Absolute fluorescence quantum yield of ligand **1** in CH_3CN.

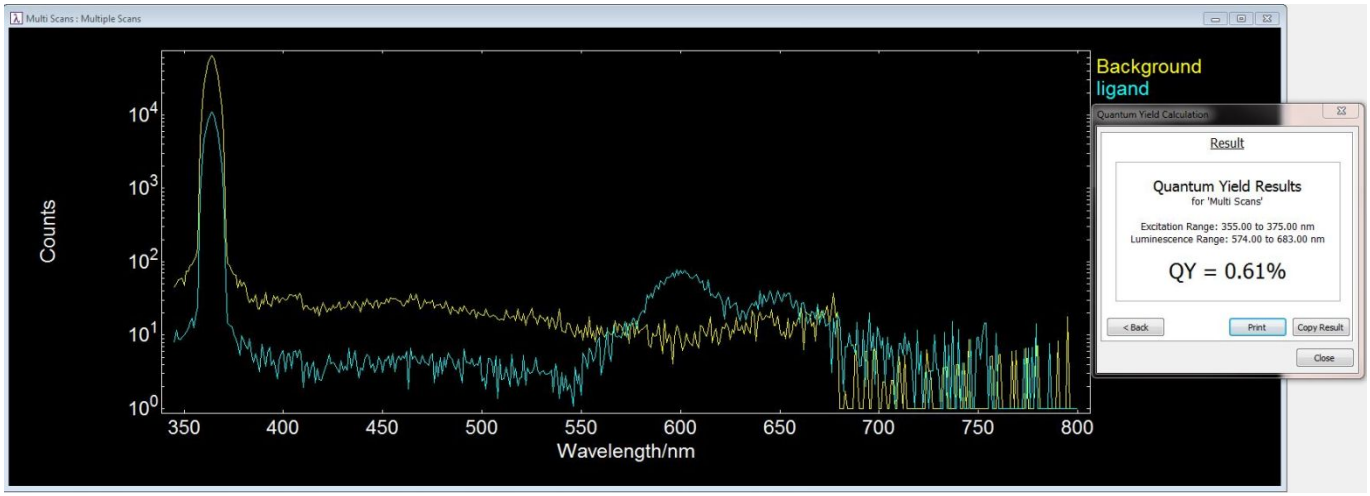

Figure S20. Absolute fluorescence quantum yield of ligand **1** in solid state.

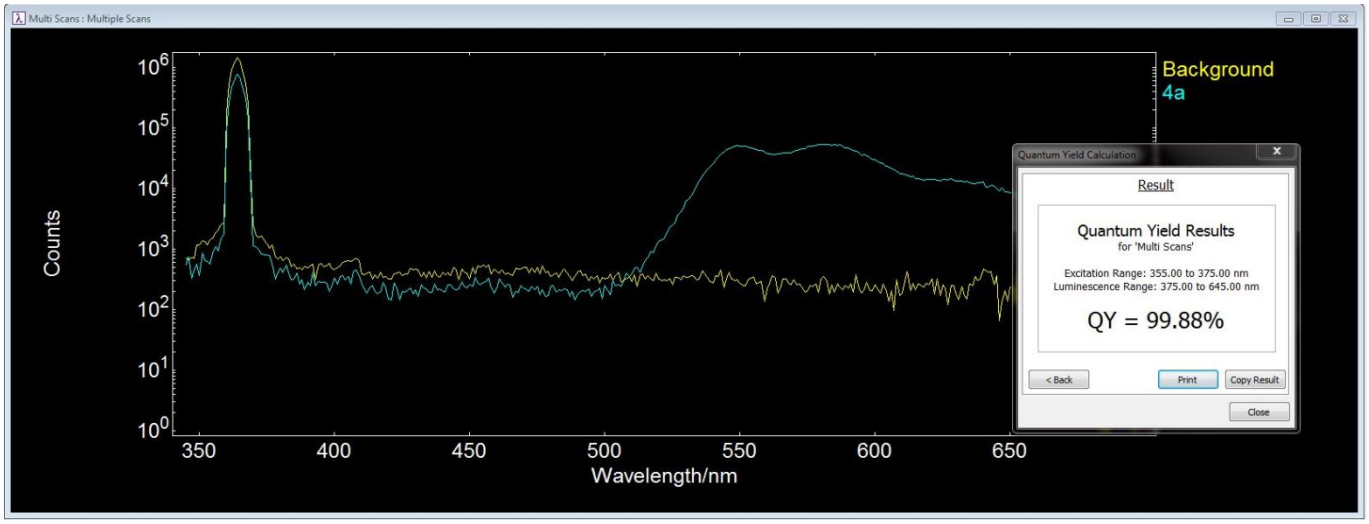

Figure S21. Absolute fluorescence quantum yield of metallacycle **4a** in CH_3CN.

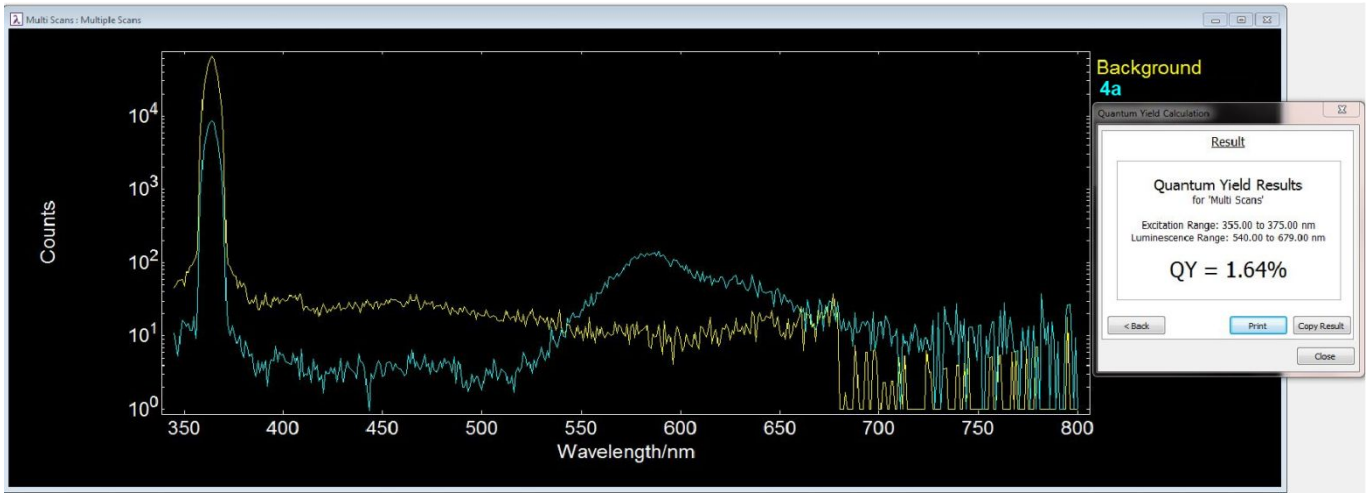

Figure S22. Absolute fluorescence quantum yield of metallacycle **4a** in solid state.

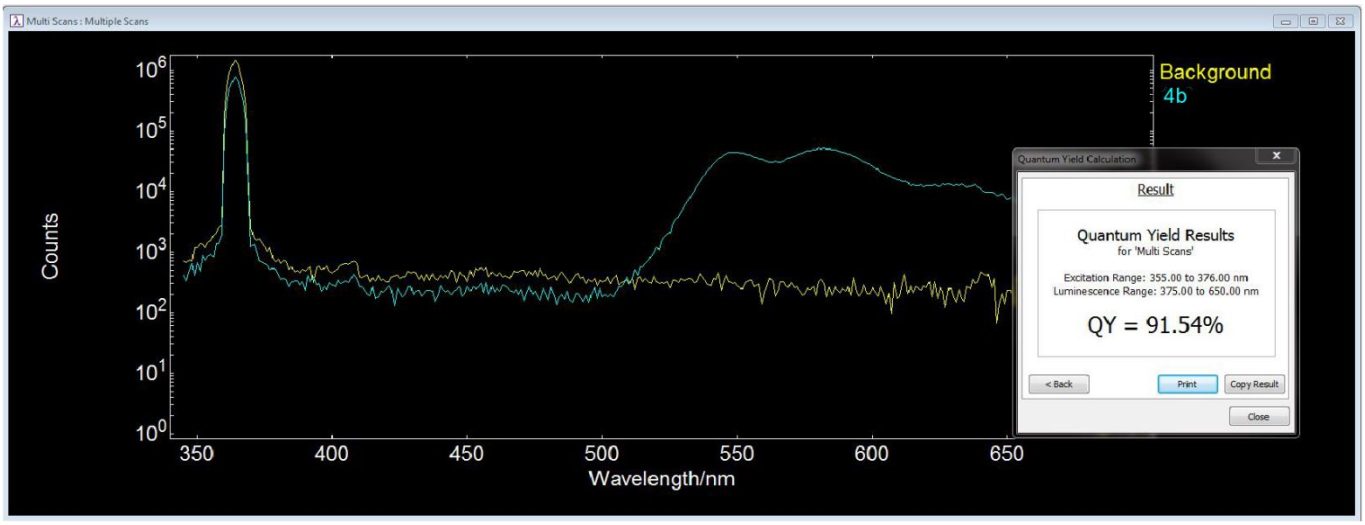

Figure S23. Absolute fluorescence quantum yield of metallacage **4b** in CH_3CN.

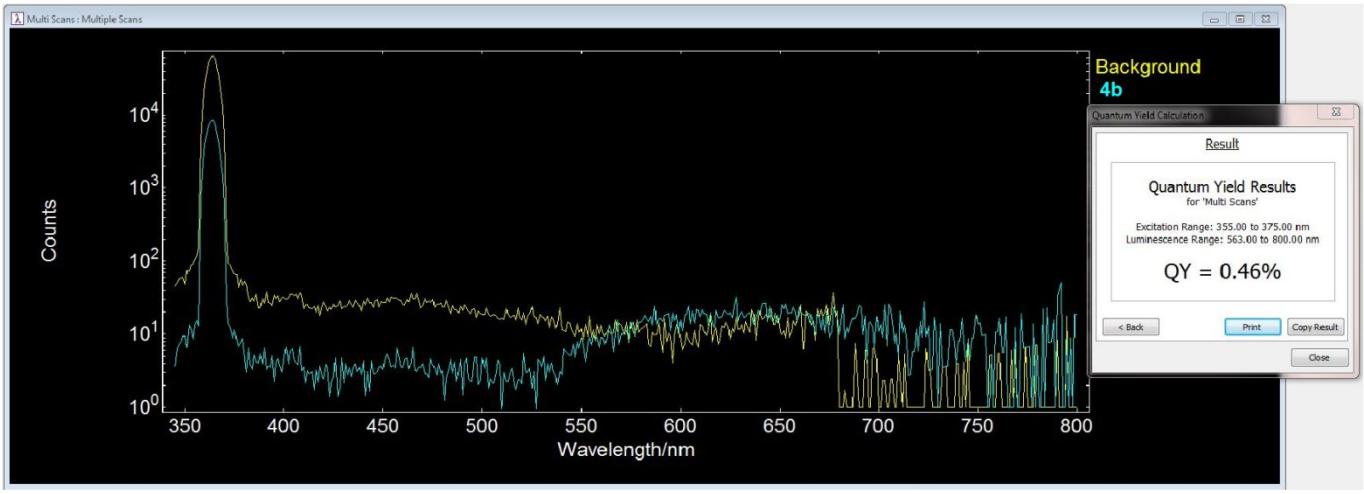

Figure S24. Absolute fluorescence quantum yield of metallacage **4b** in solid state.

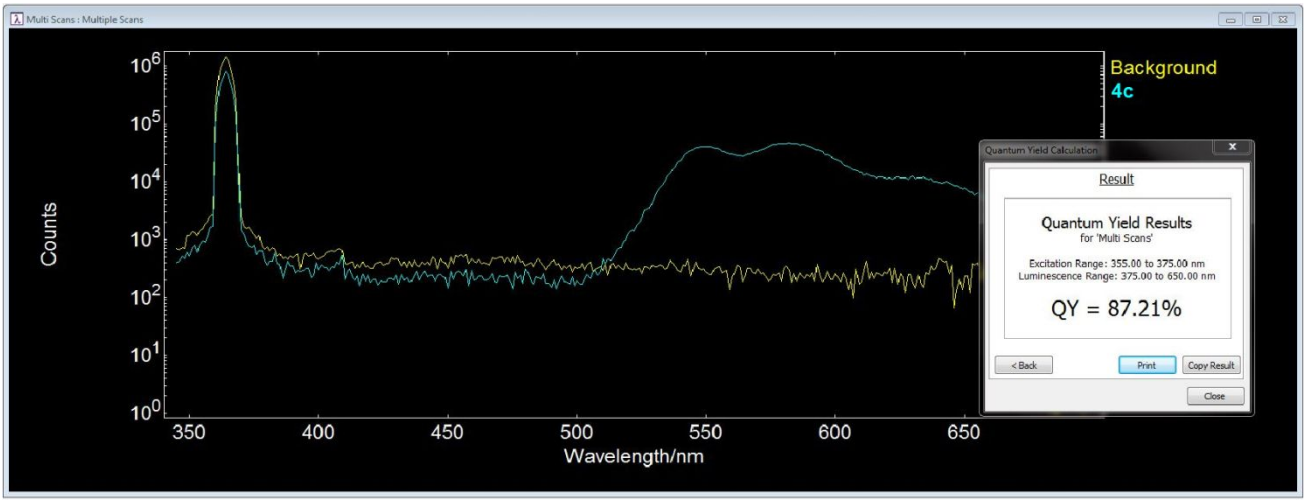

Figure S25. Absolute fluorescence quantum yield of metallacage **4c** in CH_3CN.

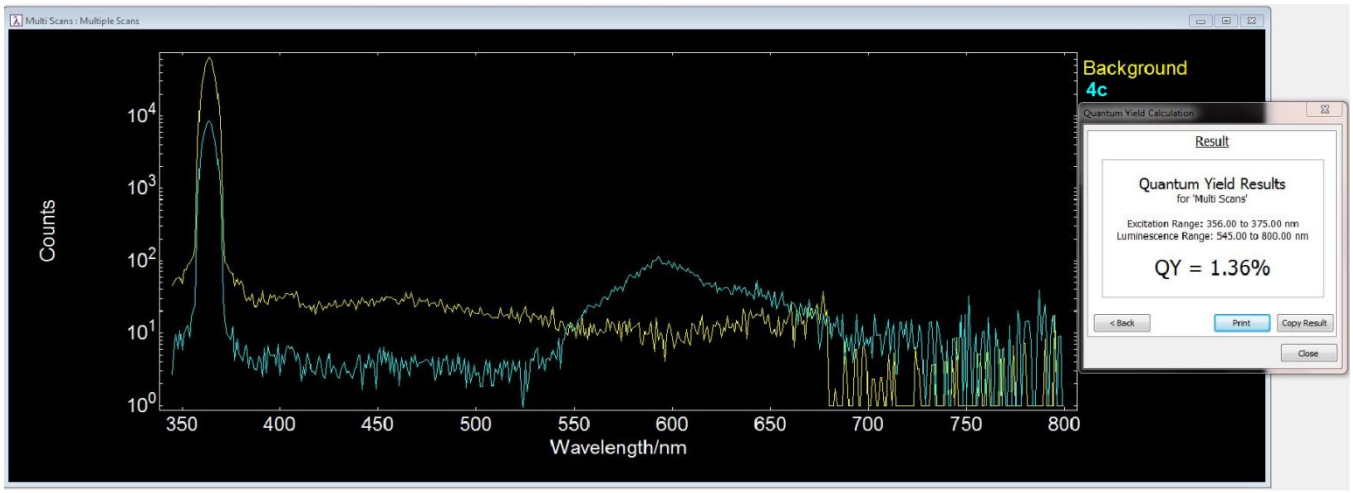

Figure S26. Absolute fluorescence quantum yield of metallacage **4c** in solid state.

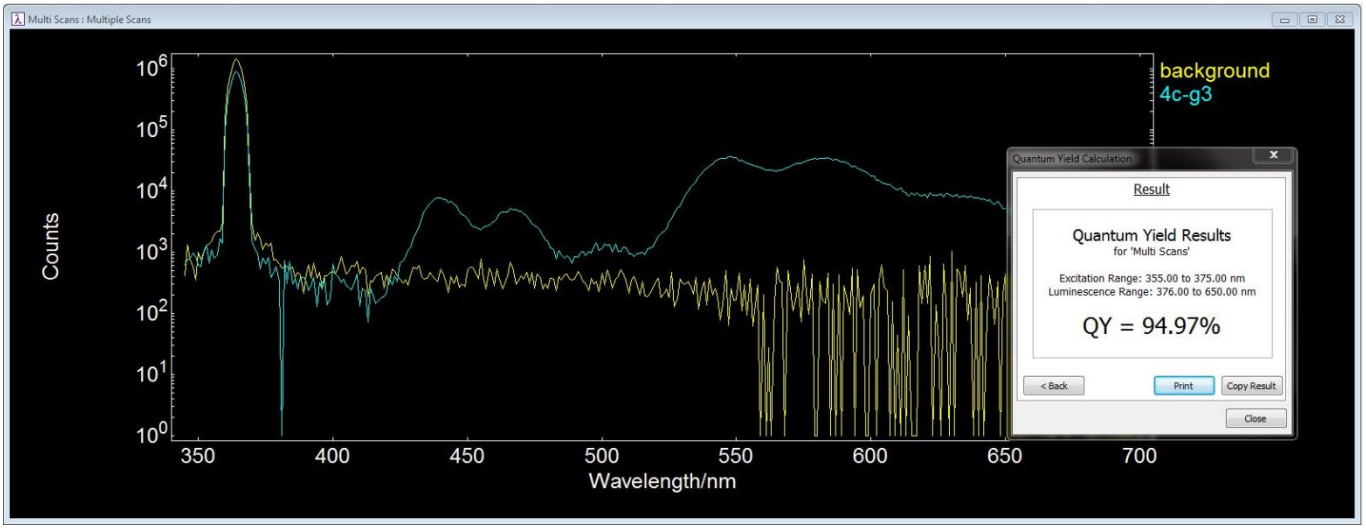

Figure S27. Absolute fluorescence quantum yield of metallacage **4c⊃G_3** in CH_3CN.

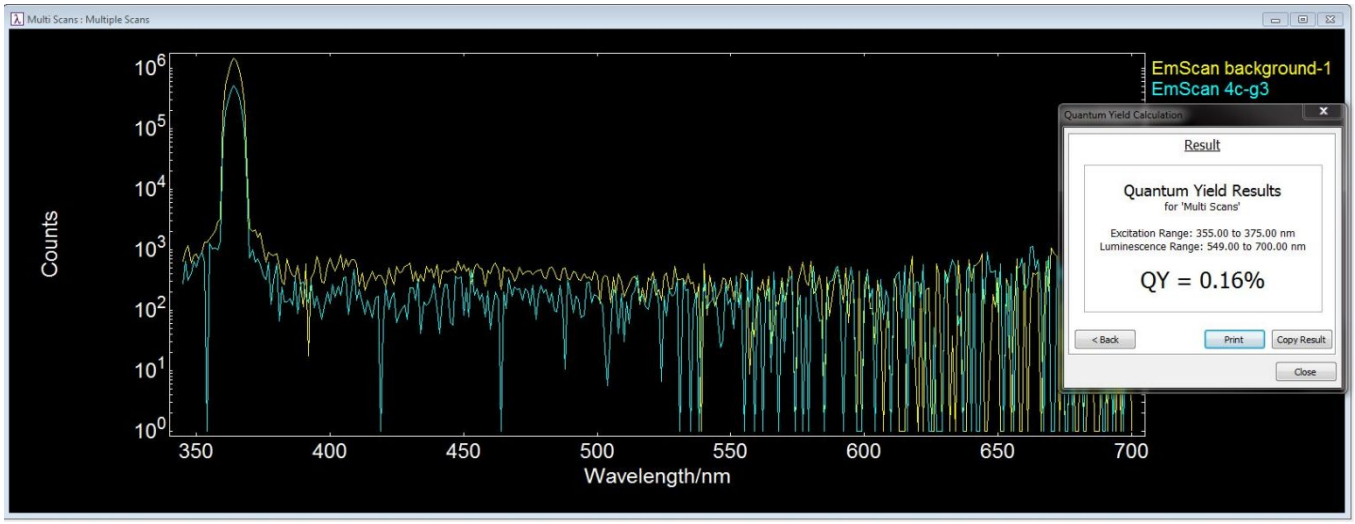

Figure S28. Absolute fluorescence quantum yield of metallacage **4c⊃G_3** in solid state.

5. Fluorescence decay traces and lifetime

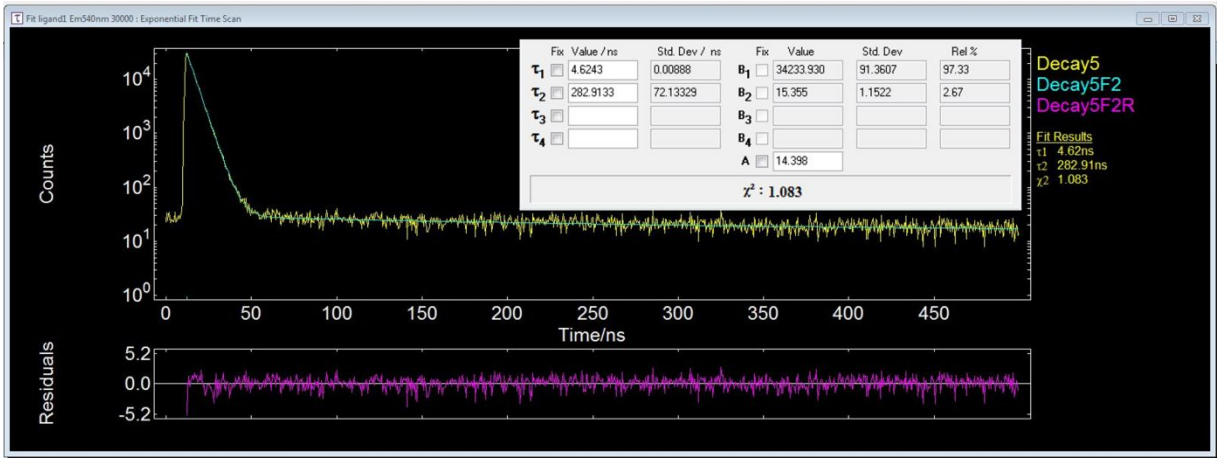

Figure S29. Fitting spectra of fluorescence decays of **1**, monitored at 540 nm with an excitation wavelength of 375 nm.

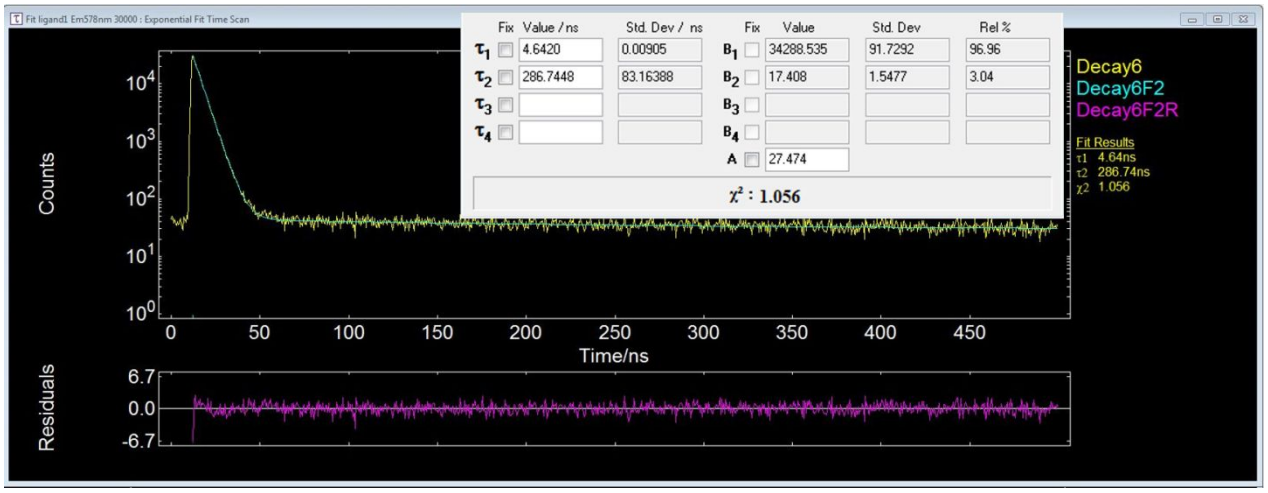

Figure S30. Fitting spectra of fluorescence decays of **1**, monitored at 578 nm with an excitation wavelength of 375 nm.

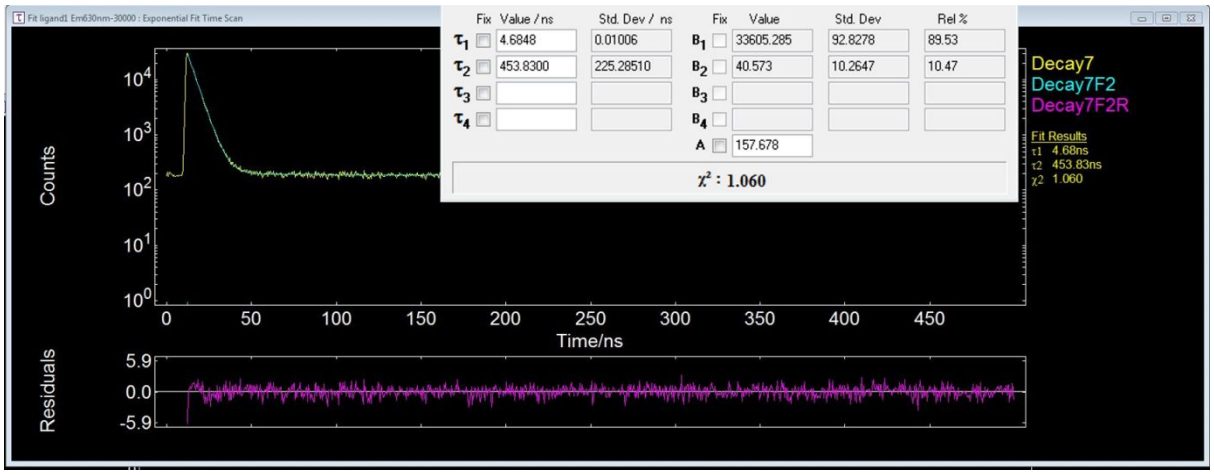

Figure S31. Fitting spectra of fluorescence decays of **4a**, monitored at 540 nm with an excitation wavelength of 375 nm.

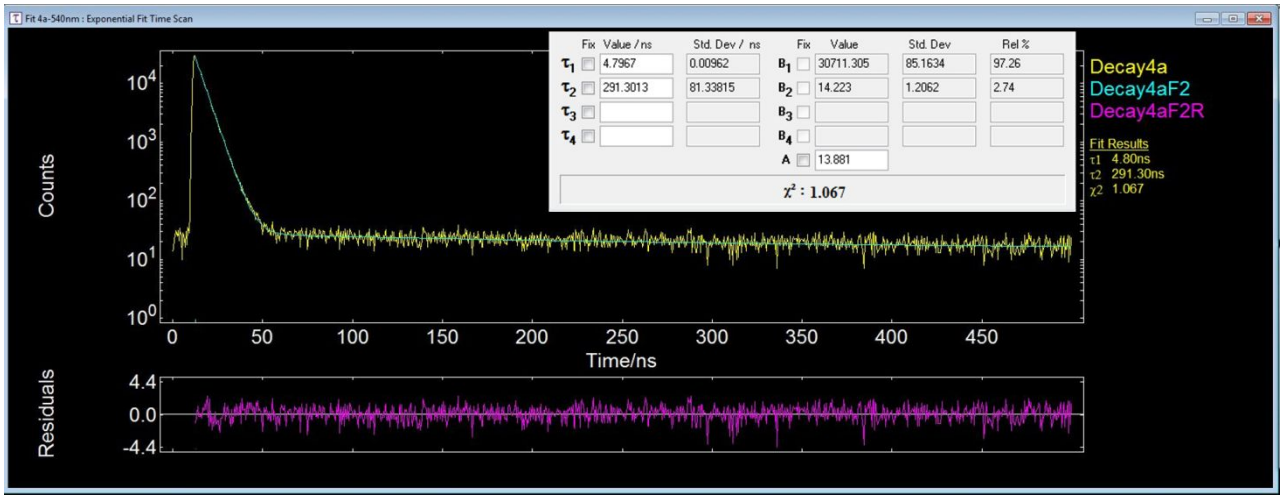

Figure S32. Fitting spectra of fluorescence decays of **4a**, monitored at 578 nm with an excitation wavelength of 375 nm.

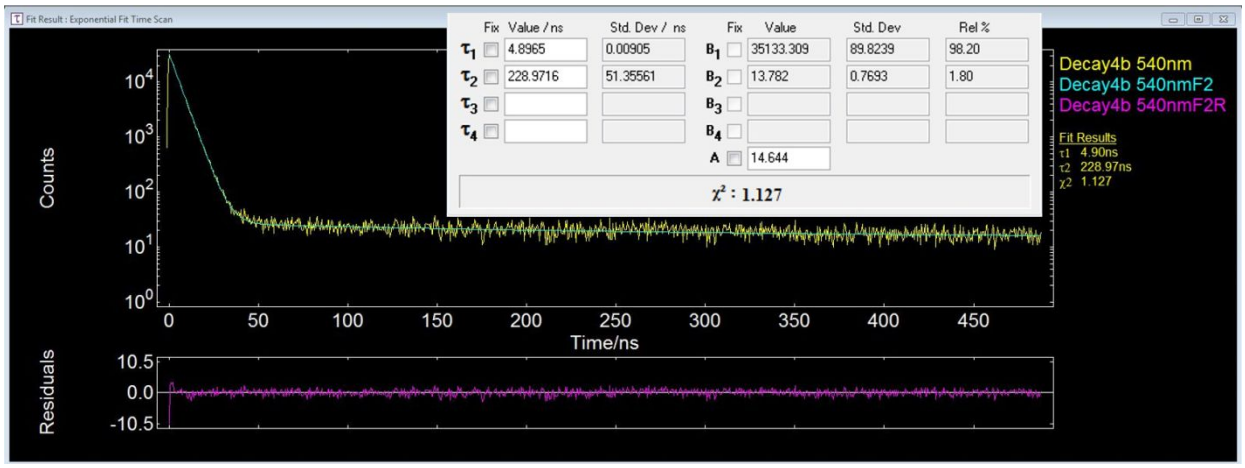

Figure S33. Fitting spectra of fluorescence decays of **4b**, monitored at 540 nm with an excitation wavelength of 375 nm.

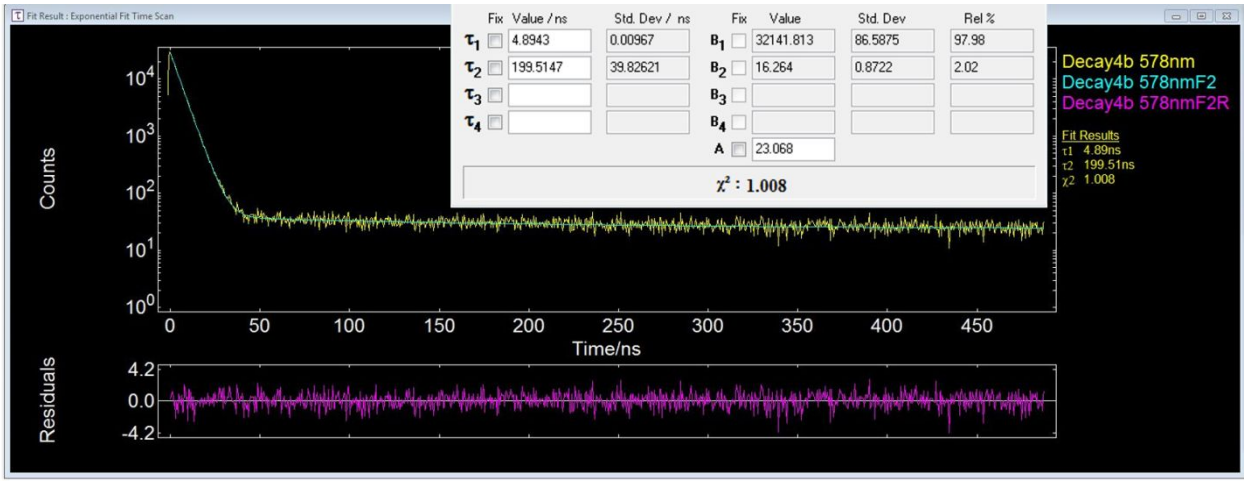

Figure S34. Fitting spectra of fluorescence decays of **4b**, monitored at 578 nm with an excitation wavelength of 375 nm.

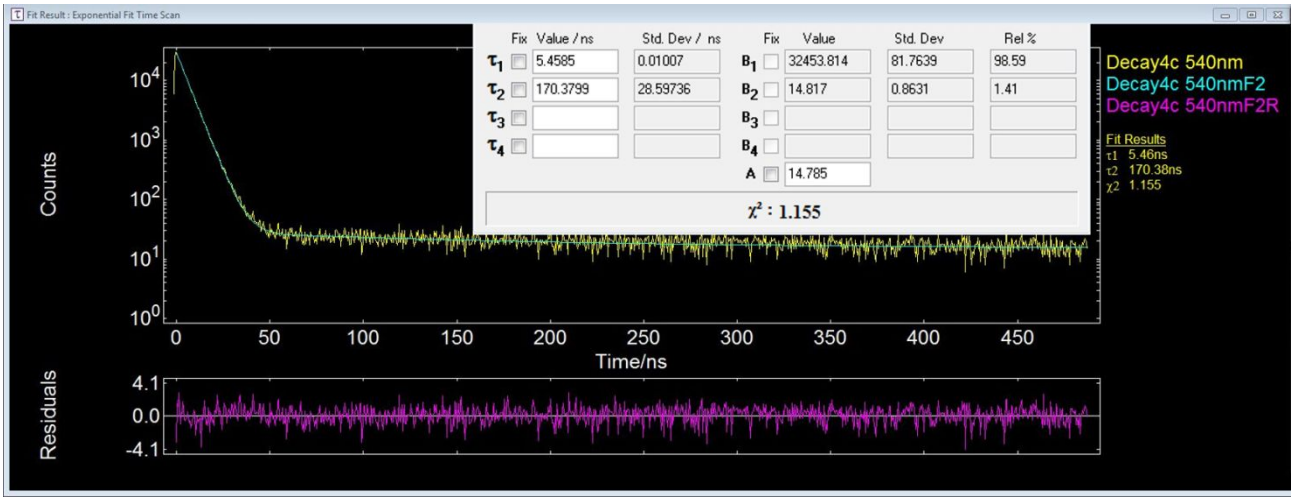

Figure S35. Fitting spectra of fluorescence decays of **4c**, monitored at 540 nm with an excitation wavelength of 375 nm.

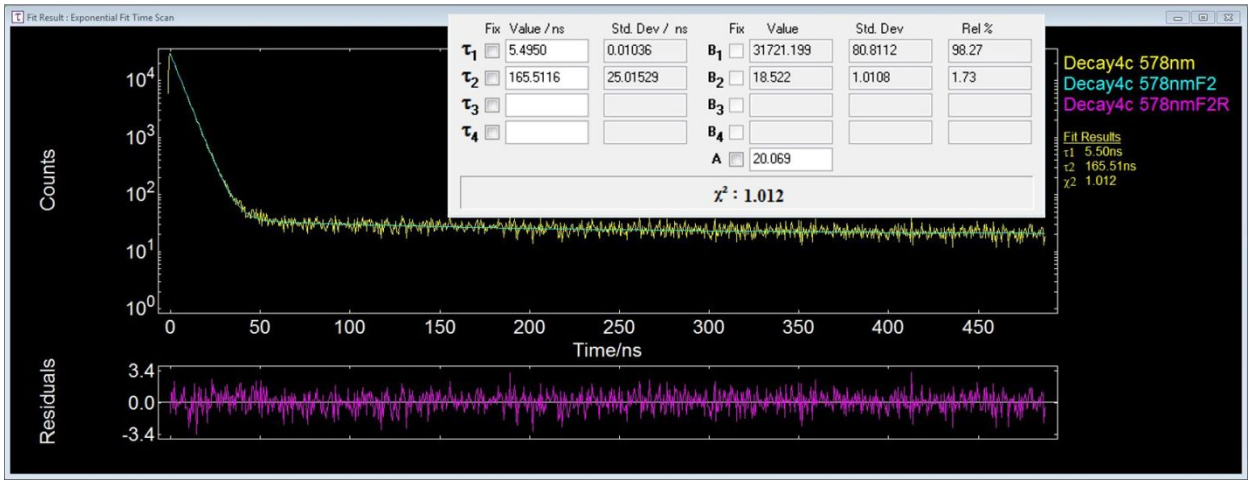

Figure S36. Fitting spectra of fluorescence decays of **4c**, monitored at 578 nm with an excitation wavelength of 375 nm.

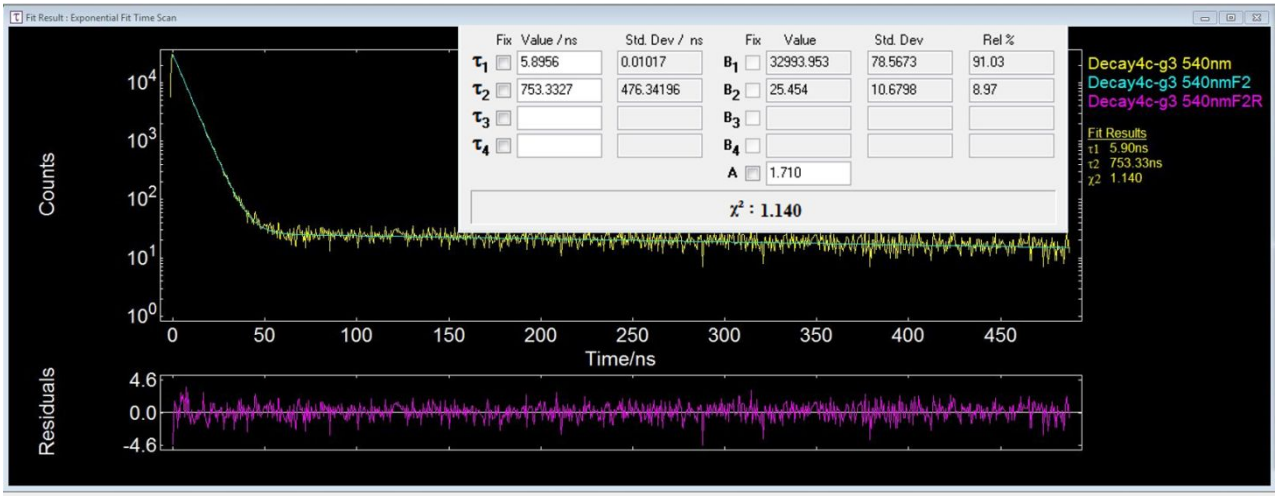

Figure S37. Fitting spectra of fluorescence decays of **4c⊃G$_3$**, monitored at 540 nm with an excitation wavelength of 375 nm.

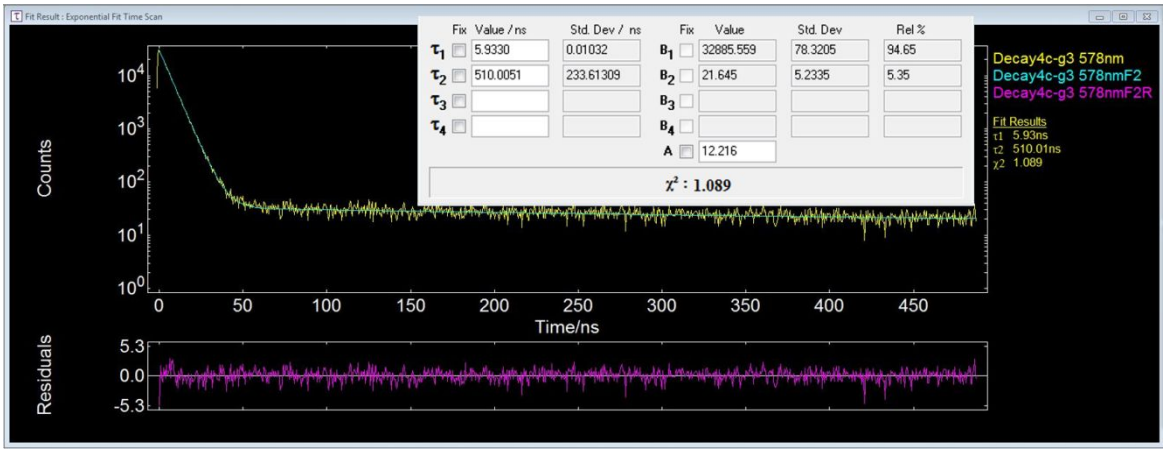

Figure S38. Fitting spectra of fluorescence decays of **4c⊃G$_3$**, monitored at 578 nm with an excitation wavelength of 375 nm.

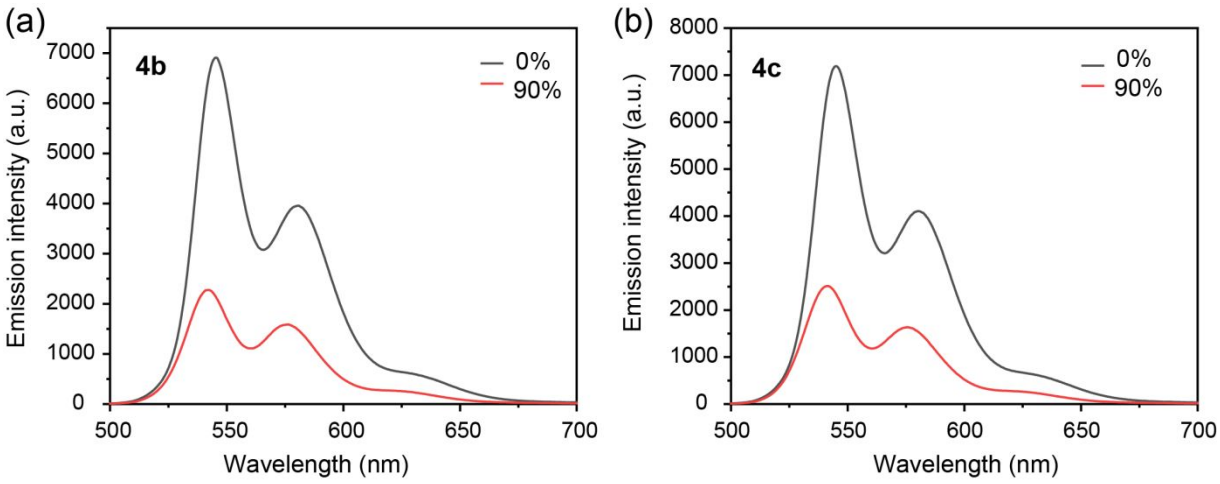

Figure S39. Emission spectra of metallacages (a) **4b** and (b) **4c** in acetonitrile with different fraction of diethyl ether.

Table S2 Fitting results of lifetime for **1**, **4a**, **4b, 4c** and **4c⊃G$_3$.**

	540 nm		578 nm	
	τ_1 (ns) and Rel	τ_2 (ns) and Rel	τ_1 (ns) and Rel	τ_2 (ns) and Rel
Ligand 1	4.62 (97.33 %)	282.91 (2.67 %)	4.64 (96.96 %)	286.75 (3.04 %)
4a	4.79 (97.26 %)	291.30 (2.74 %)	4.80 (97.37 %)	233.06 (2.63 %)
4b	4.90 (98.20 %)	228.97 (1.80%)	4.89 (97.98 %)	199.51 (2.02 %)
4c	5.45 (98.59 %)	170.38 (1.41%)	5.49 (98.27 %)	165.51 (1.73 %)
4c⊃ G$_3$	5.90 (91.03 %)	753.33 (8.97 %)	5.93 (94.65 %)	510.00 (5.35 %)

6. Host-guest complexation study

6.1 Determination of stoichiometry by UV-vis absorption spectra

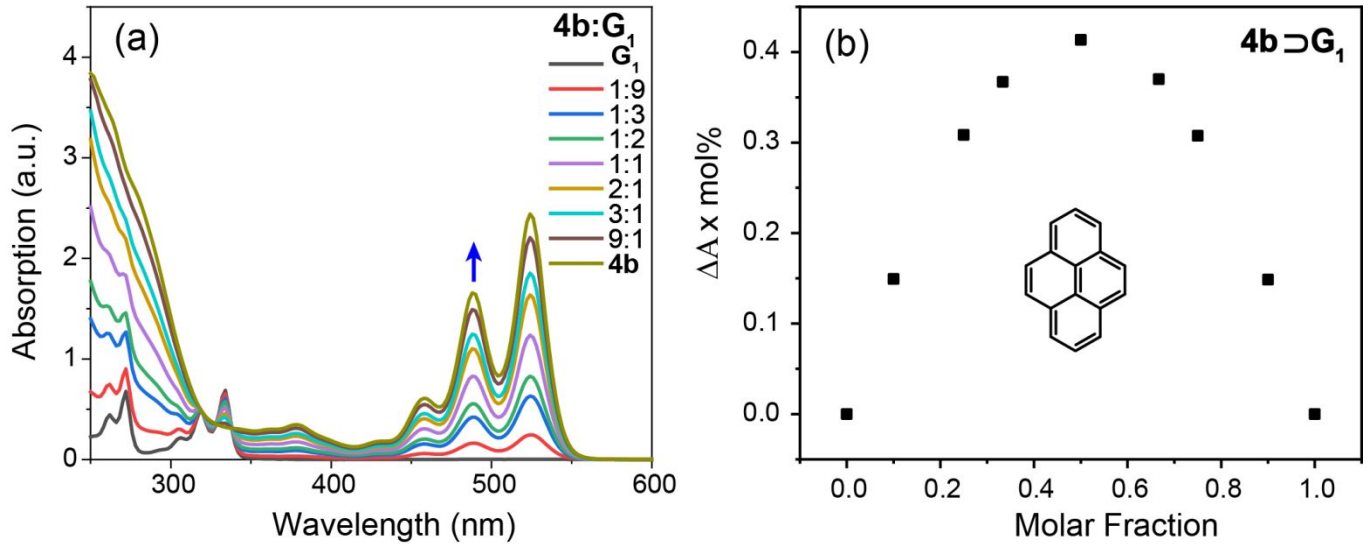

Figure S40. (a) UV-vis absorption of metallacage **4b** with guest $\mathbf{G_1}$ in different molar ratios ([**4b**] + [$\mathbf{G_1}$] = 10 μM). (b) Job's plot of the complex **4b**⊃$\mathbf{G_1}$ in CH_3CN, showing a 1:1 stoichiometry.

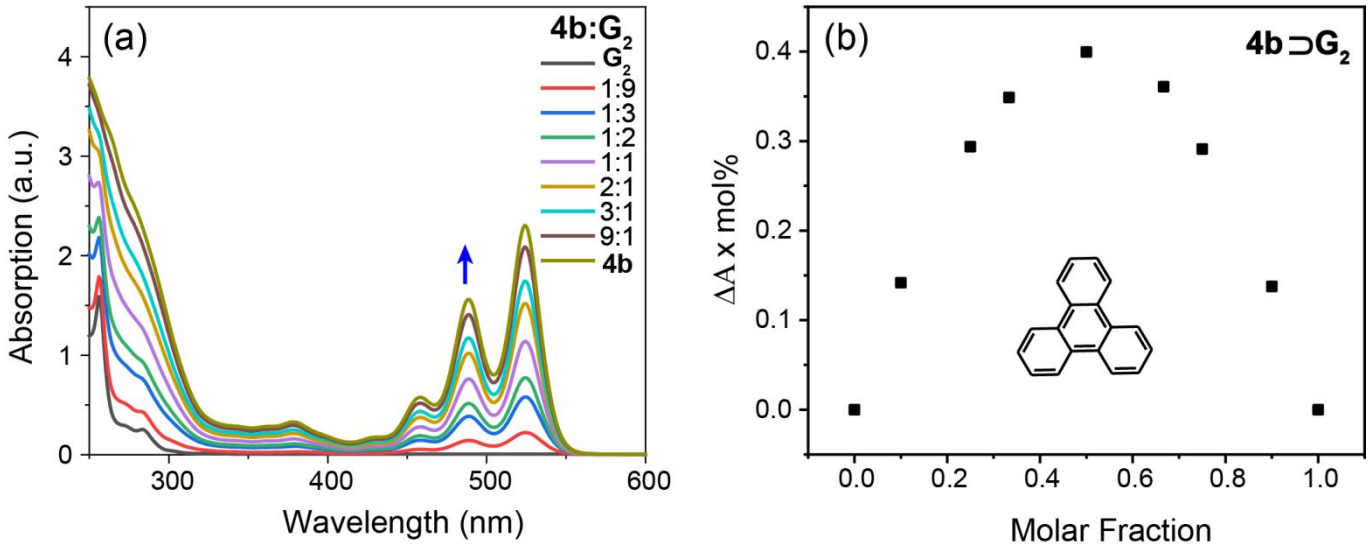

Figure S41. (a) UV-vis absorption of metallacage **4b** with guest $\mathbf{G_2}$ in different molar ratios ([**4b**] + [$\mathbf{G_2}$] = 10 μM). (b) Job's plot of the complex **4b**⊃$\mathbf{G_2}$ in CH_3CN, showing a 1:1 stoichiometry.

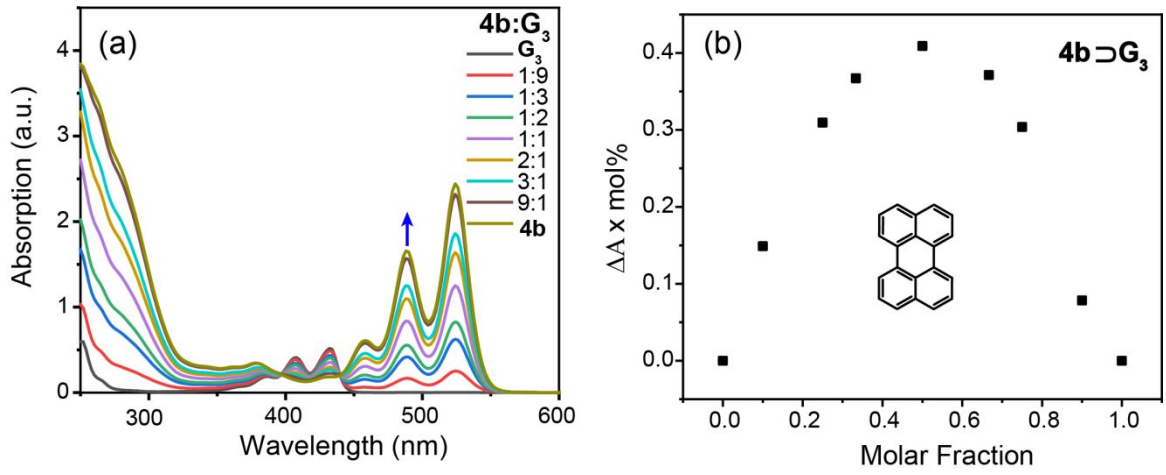

Figure S42. (a) UV-vis absorption of metallacage **4b** with guest $\mathbf{G_3}$ in different molar ratios ([**4b**] + [$\mathbf{G_3}$] = 10 μM). (b) Job's plot of the complex **4b**⊃$\mathbf{G_3}$ in CH_3CN, showing a 1:1 stoichiometry.

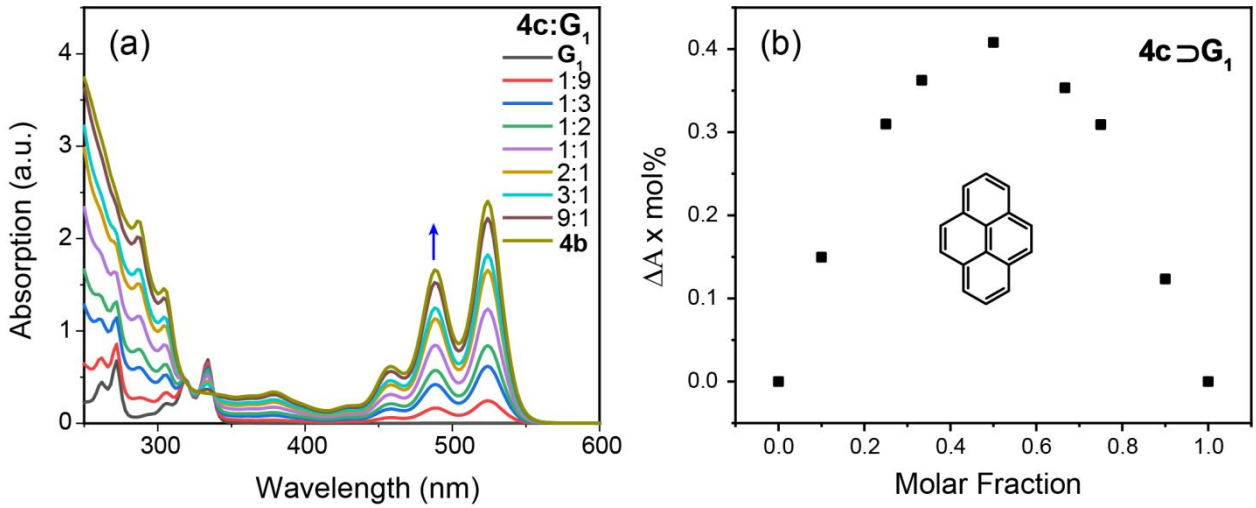

Figure S43. (a) UV-vis absorption of metallacage **4c** with guest $\mathbf{G_1}$ in different molar ratios ([**4c**] + [$\mathbf{G_1}$] = 10 μM). (b) Job's plot of the complex **4c**⊃$\mathbf{G_1}$ in CH_3CN, showing a 1:1 stoichiometry.

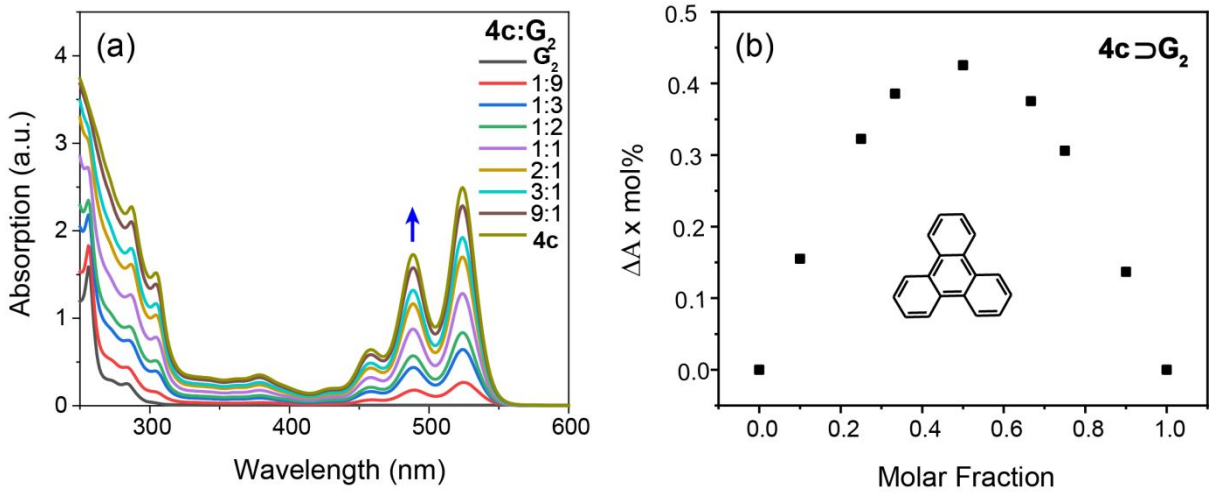

Figure S44. (a) UV-vis absorption of metallacage **4c** with guest $\mathbf{G_2}$ in different molar ratios ([**4c**] + [$\mathbf{G_2}$] = 10 μM). (b) Job's plot of the complex **4c**⊃$\mathbf{G_2}$ in CH_3CN, showing a 1:1 stoichiometry.

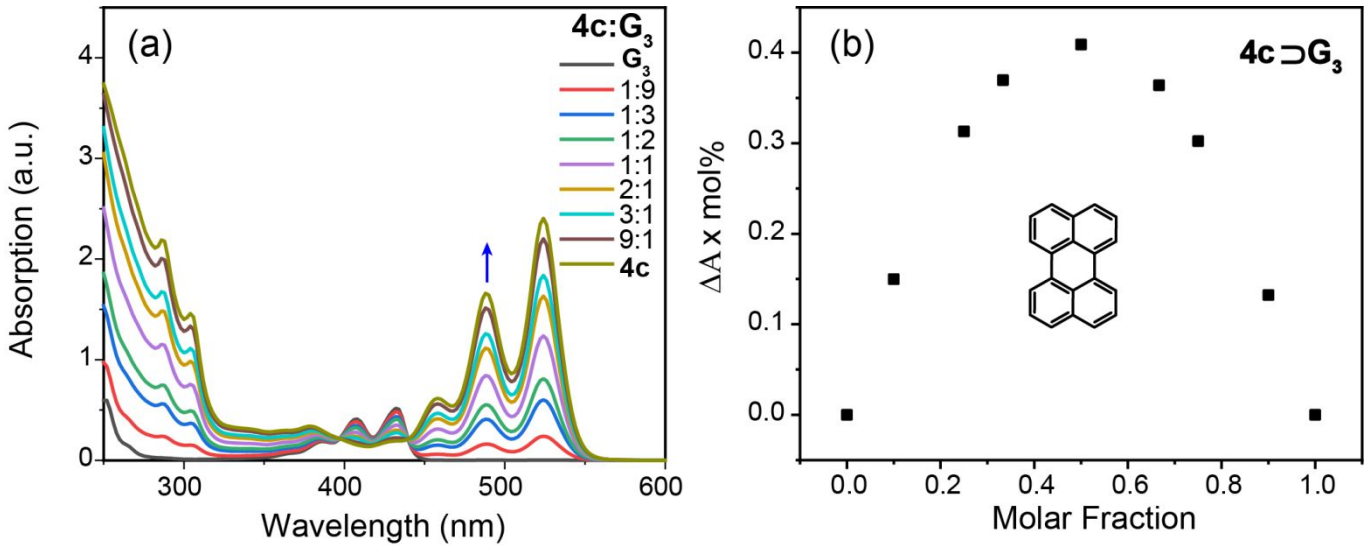

Figure S45. (a) UV-vis absorption of metallacage **4c** with guest $\mathbf{G_3}$ in different molar ratios ([**4c**] + [$\mathbf{G_3}$] = 10 μM). (b) Job's plot of the complex **4c**⊃$\mathbf{G_3}$ in CH_3CN, showing a 1:1 stoichiometry.

6.2 ESI-TOF-MS spectra of complexes

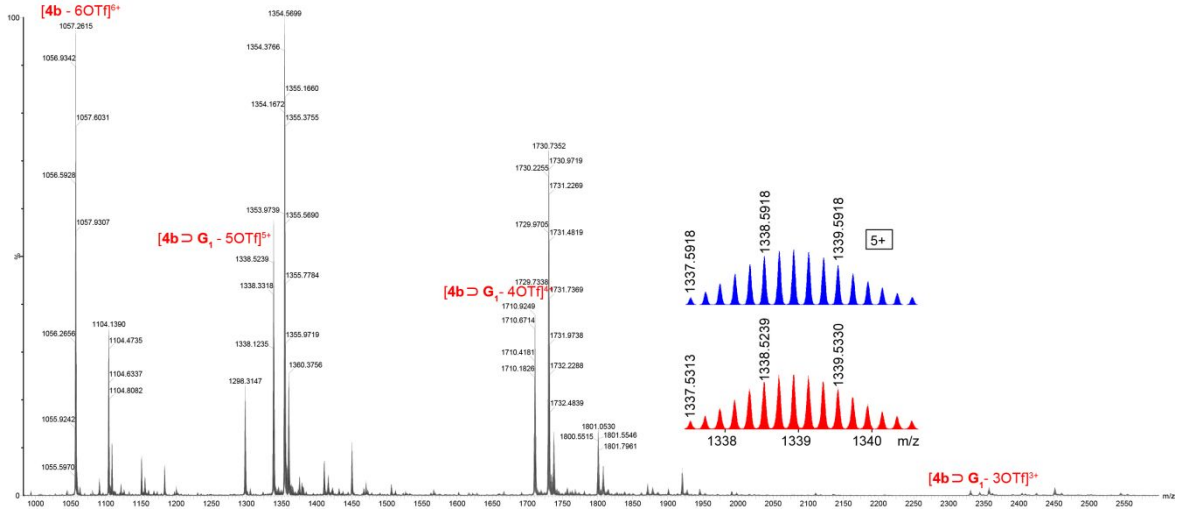

Figure S46. ESI-TOF-MS spectrum of complex **4b**⊃$\mathbf{G_1}$.

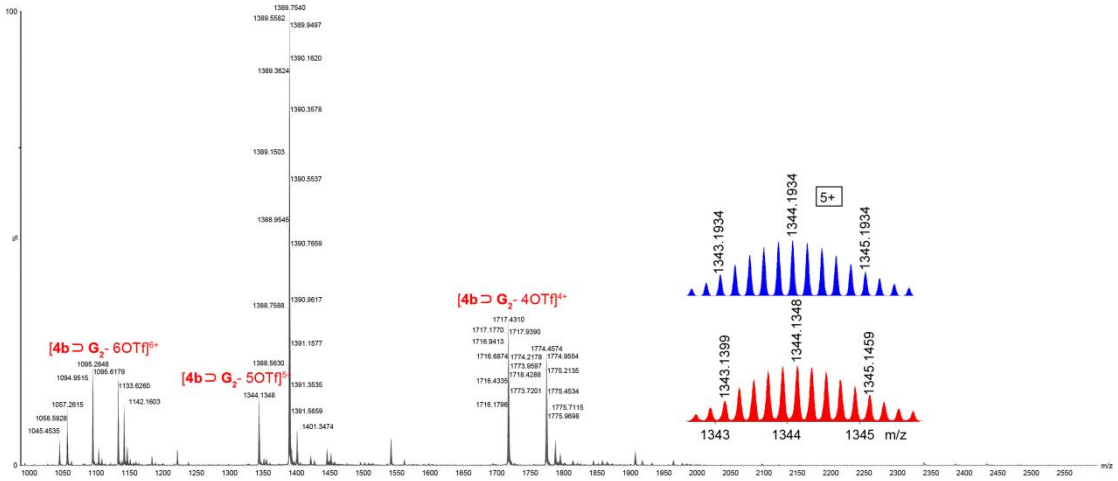

Figure S47. ESI-TOF-MS spectrum of complex **4b**⊃$\mathbf{G_2}$.

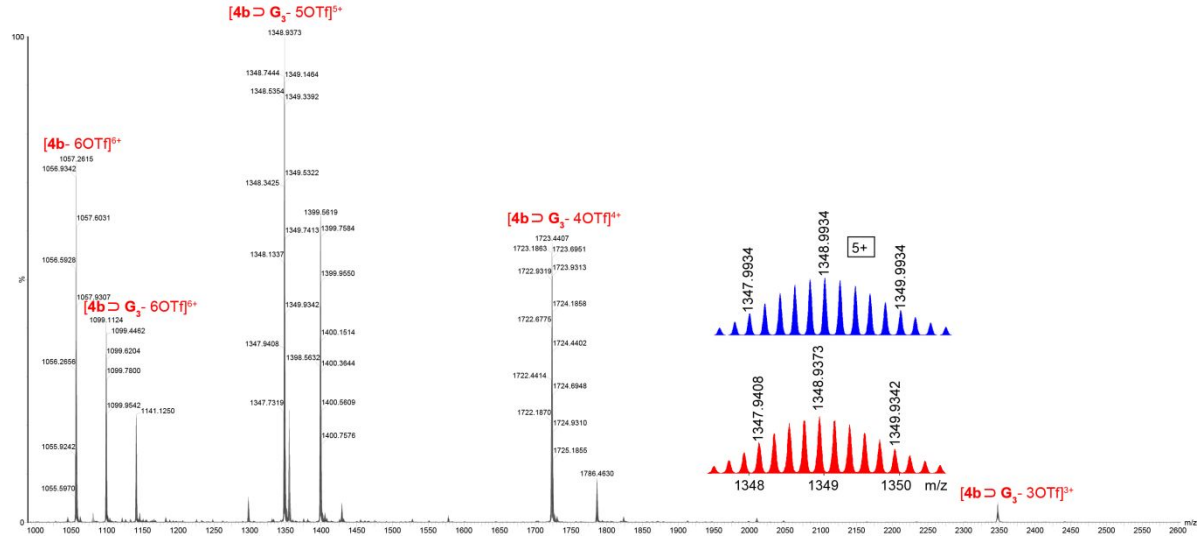

Figure S48. ESI-TOF-MS spectrum of complex **4b⊃G$_3$**.

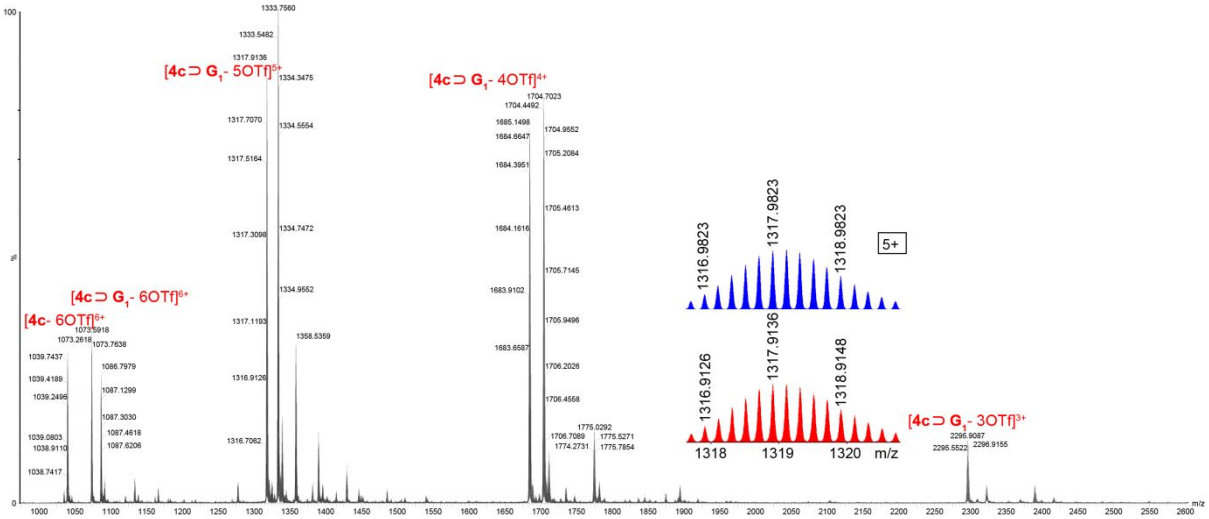

Figure S49. ESI-TOF-MS spectrum of complex **4c⊃G$_1$**.

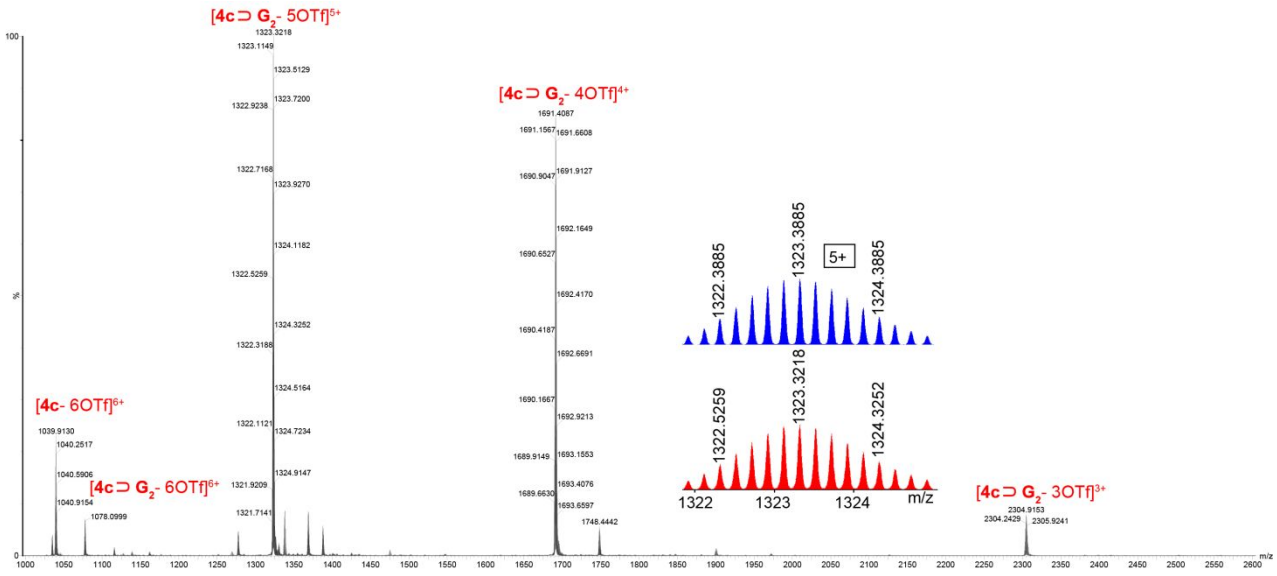

Figure S50. ESI-TOF-MS spectrum of complex **4c⊃G$_2$**.

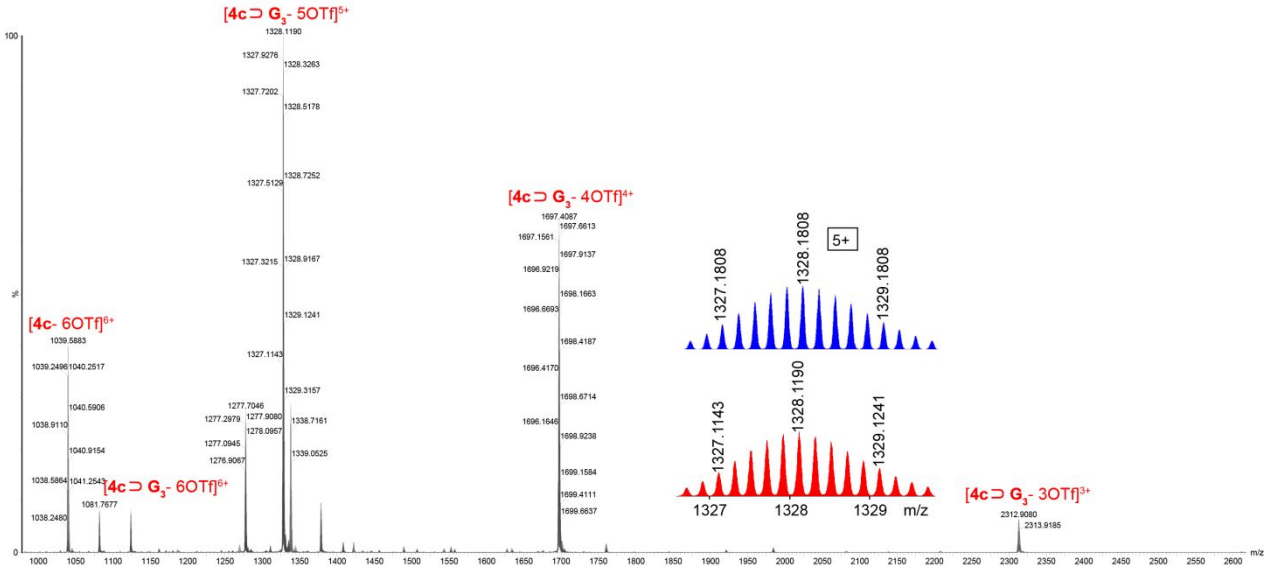

Figure S51. ESI-TOF-MS spectrum of complex **4c⊃G$_3$**.

6.3 Determination of binding constant (K_a) by ^{1}H NMR titration method

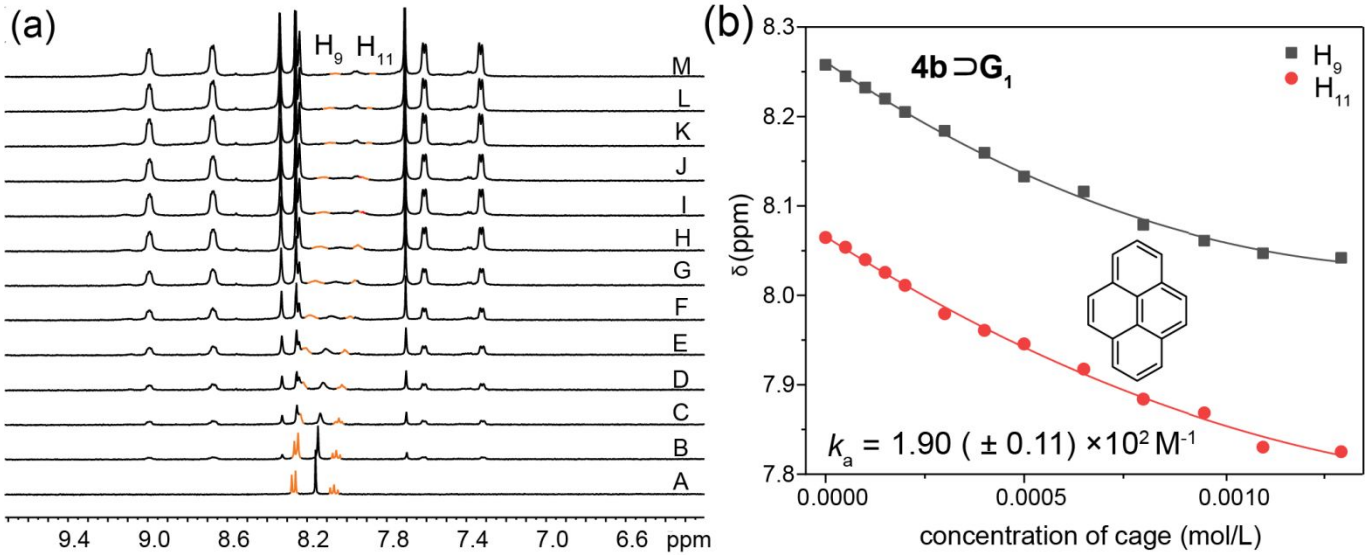

Figure S52. ^{1}H NMR spectra (400 MHz, CD_3CN, 295 K) of **G$_1$** at the fixed concentration of 0.5 mM upon the addition of metallacage **4b**: (A) 0 mM, (B) 0.05 mM, (C) 0.10 mM, (D) 0.15 mM, (E) 0.20 mM, (F) 0.30 mM, (G) 0.40 mM, (H) 0.50 mM, (I) 0.65 mM, (J) 0.8 mM, (K)0.95 mM, (L) 1.10 mM, (M) 1.30 mM.

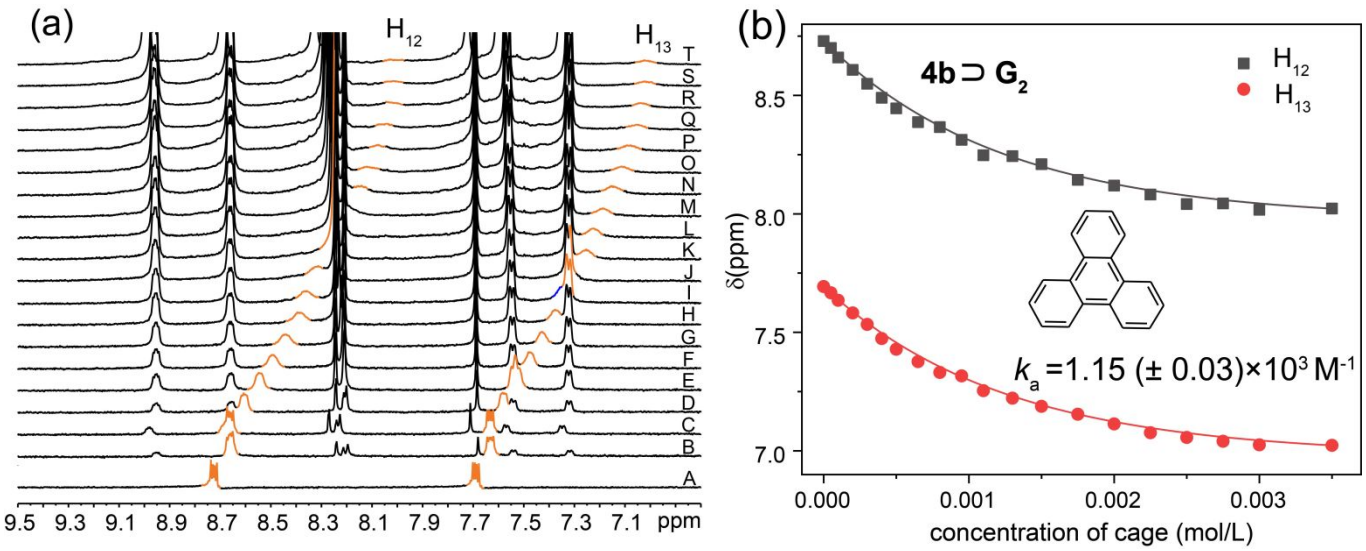

Figure S53. ^{1}H NMR spectra (400 MHz, CD_3CN, 295 K) of $\mathbf{G_2}$ at the fixed concentration of 0.5 mM upon the addition of metallacage **4b**: (A) 0 mM, (B) 0.05 mM, (C) 0.10 mM, (D) 0.15 mM, (E) 0.20 mM, (F) 0.30 mM, (G) 0.40 mM, (H) 0.50 mM, (I) 0.65 mM, (J) 0.8 mM, (K) 1.10 mM, (L) 1.30 mM, (M) 1.50 mM, (N) 1.75 mM, (O) 2.00 mM, (P) 2.25 mM, (Q) 2.50 mM, (R) 2.75 mM, (S) 3.00 mM, (T) 3.50 mM.

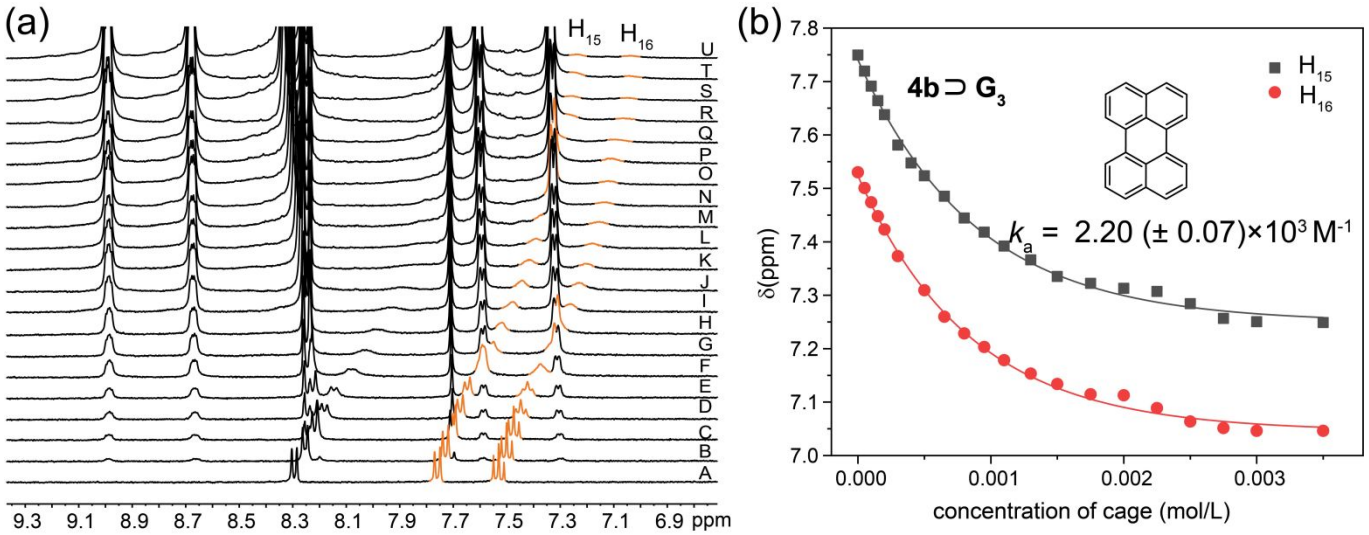

Figure S54. ^{1}H NMR spectra (400 MHz, CD_3CN, 295 K) of $\mathbf{G_3}$ at the fixed concentration of 0.5 mM upon the addition of metallacage **4b**: (A) 0 mM, (B) 0.05 mM, (C) 0.10 mM, (D) 0.15 mM, (E) 0.20 mM, (F) 0.30 mM, (G) 0.40 mM, (H) 0.50 mM, (I) 0.65 mM, (J) 0.8 mM, (K)0.95 mM, (L) 1.10 mM, (M) 1.30 mM, (N) 1.50 mM, (O) 1.75 mM, (P) 2.00 mM, (Q) 2.25 mM, (R) 2.50 mM, (S) 2.75 mM, (T) 3.00 mM, (U) 3.50 mM.

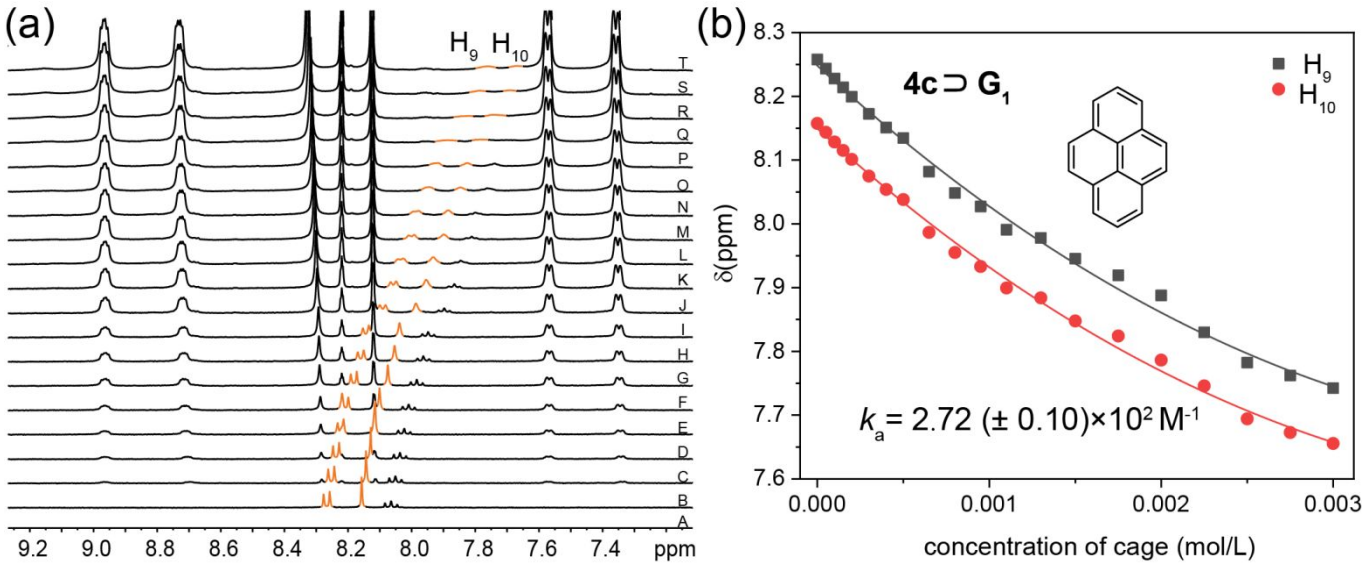

Figure S55. ^{1}H NMR spectra (400 MHz, CD_3CN, 295 K) of $\mathbf{G_1}$ at the fixed concentration of 0.5 mM upon the addition of metallacage **4c**: (A) 0 mM, (B) 0.05 mM, (C) 0.10 mM, (D) 0.15 mM, (E) 0.20 mM, (F) 0.30 mM, (G) 0.40 mM, (H) 0.50 mM, (I) 0.65 mM, (J) 0.8 mM, (K)0.95 mM, (L) 1.10 mM, (M) 1.30 mM, (N) 1.50 mM, (O) 1.75 mM, (P) 2.00 mM, (Q) 2.25 mM, (R) 2.50 mM, (S) 2.75 mM, (T) 3.00 mM.

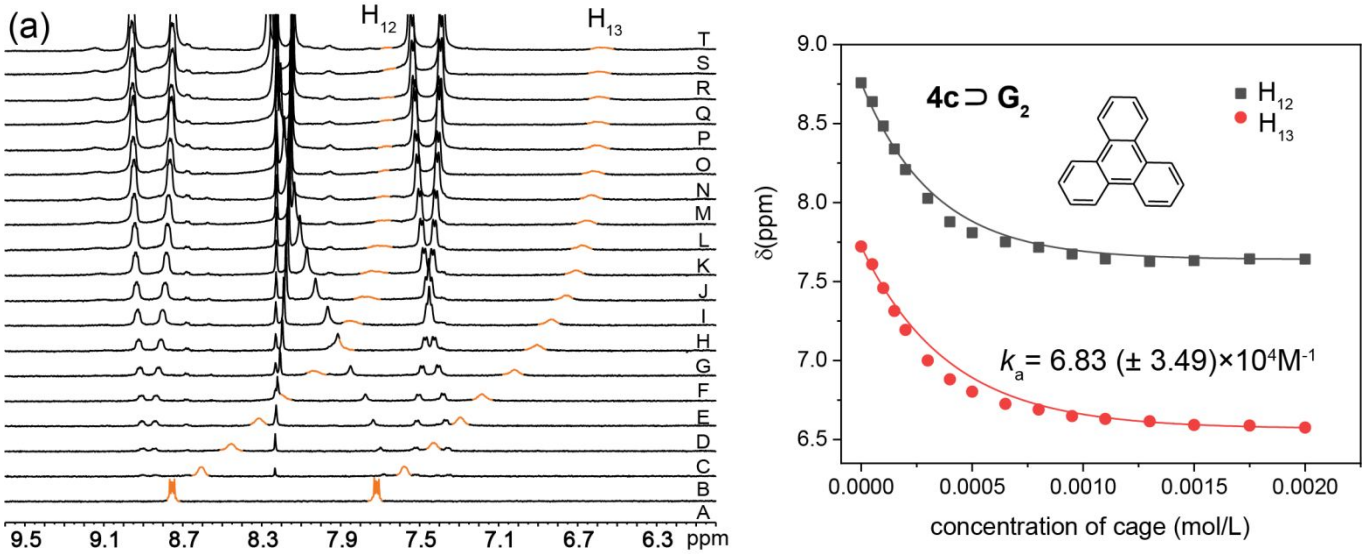

Figure S56. ^{1}H NMR spectra (400 MHz, CD_3CN, 295 K) of $\mathbf{G_2}$ at the fixed concentration of 0.5 mM upon the addition of metallacage **4c**: (A) 0 mM, (B) 0.05 mM, (C) 0.10 mM, (D) 0.15 mM, (E) 0.20 mM, (F) 0.30 mM, (G) 0.40 mM, (H) 0.50 mM, (I) 0.65 mM, (J) 0.8 mM, (K)0.95 mM, (L) 1.10 mM, (M) 1.30 mM, (N) 1.50 mM, (O) 1.75 mM, (P) 2.00 mM, (Q) 2.25 mM, (R) 2.50 mM, (S) 2.75 mM, (T) 3.00 mM.

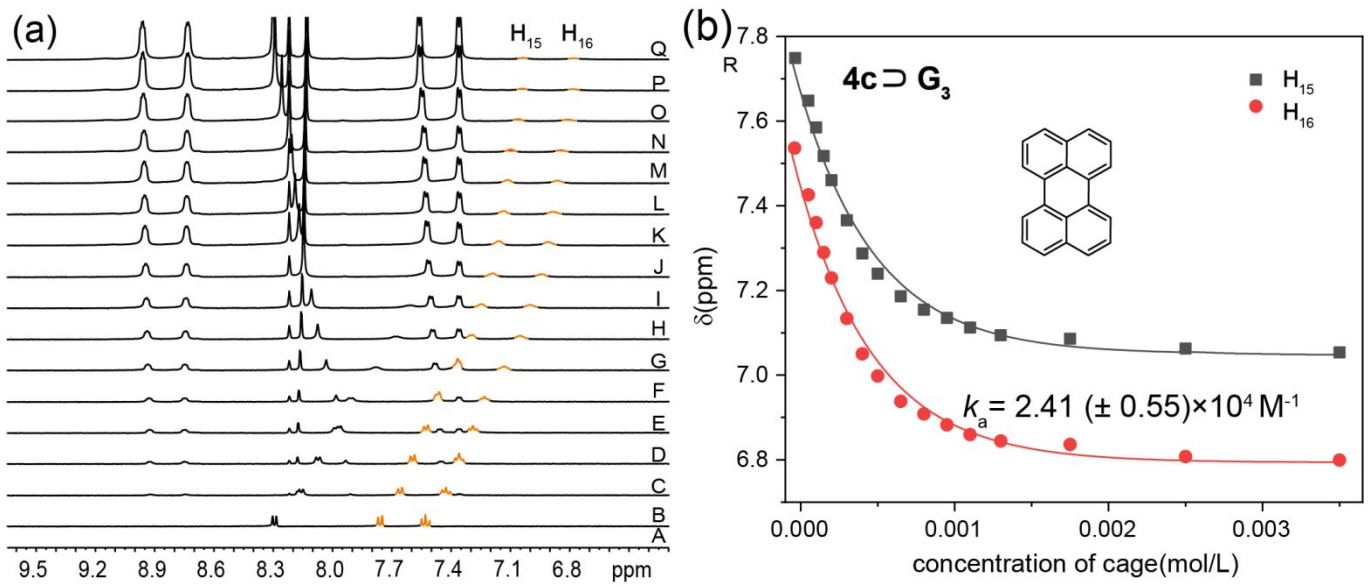

Figure S57. ^{1}H NMR spectra (400 MHz, CD_3CN, 295 K) of $\mathbf{G_3}$ at the fixed concentration of 0.5 mM upon the addition of metallacage **4c**: (A) 0 mM, (B) 0.05 mM, (C) 0.10 mM, (D) 0.15 mM, (E) 0.20 mM, (F) 0.30 mM, (G) 0.40 mM, (H) 0.50 mM, (I) 0.65 mM, (J) 0.8 mM, (K)0.95 mM, (L) 1.10 mM, (M) 1.30 mM, (N) 1.50 mM, (O) 1.75 mM, (P) 2.25 mM, (Q) 3.50 mM.

7. The fluorescence spectra and corresponding CIE coordinates of complex ***4c⊃G₃***

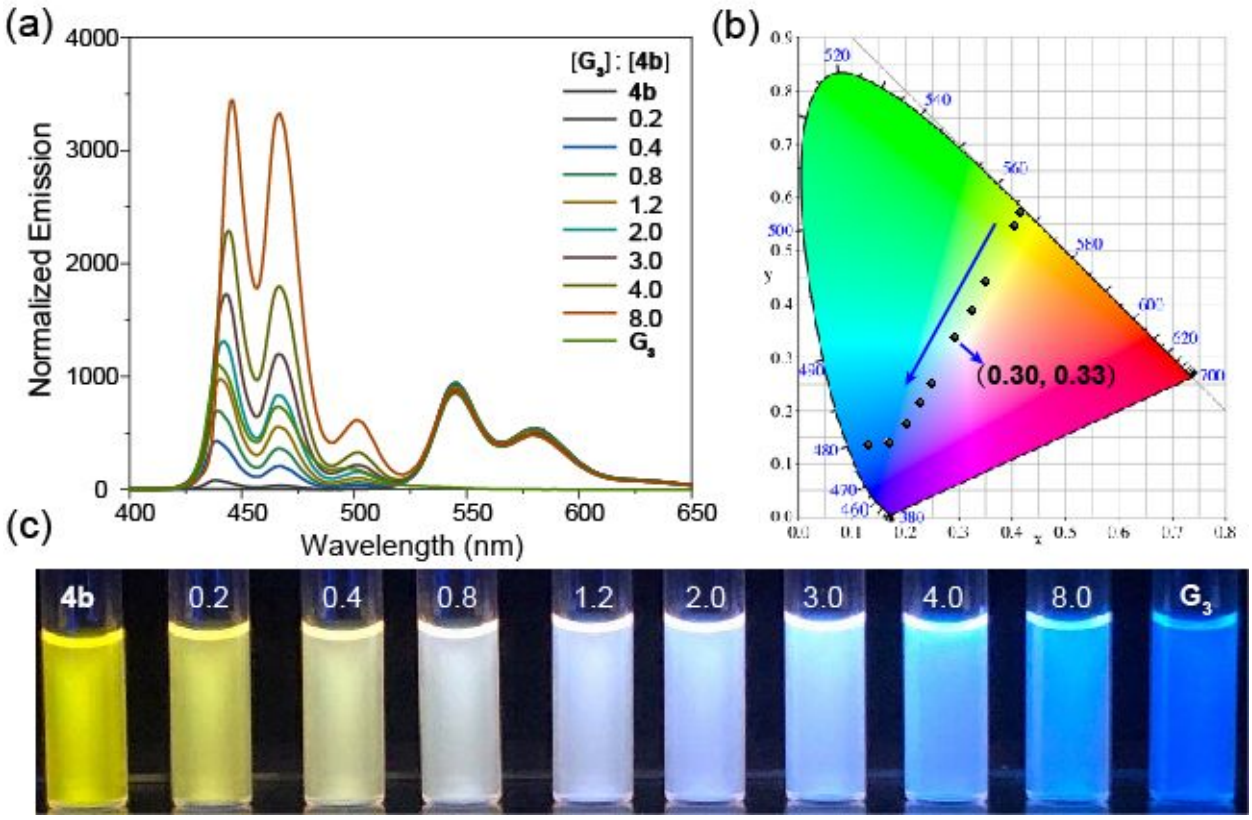

Figure S58. (a) Emission spectra of metallacage **4b** with increasing amount of $\mathbf{G_3}$, (b) their corresponding 1931 CIE chromaticity coordinates and (c) fluorescence photographs in CH_3CN. ([**4b**] = 10 μM, λ_{ex} = 365 nm, 295 K).

References

S1. Takuro Teraoka, S. H., and Hiroshi Shinokubo, Iridium-Catalyzed Direct Tetraborylation of Perylene Bisimides. *Org. Lett*. **2011**, *13*, 2532.

S2. Zheng, Y.; Zhao, Z.; Wang, M.; Ghosh, K.; Pollock, J. B.; Cook, T. R.; Stang, P. J. A Facile Approach toward Multicomponent Supramolecular Structures: Selective Self-Assembly via Charge Separation. *J. Am. Chem. Soc.* **2010**, *132*, 16873.

S3. http://app.supramolecular.org/bindfit/